*future pharmacology*

MDPI

*Article*

# Discovery of Arylfuran and Carbohydrate Derivatives from the BraCoLi Library as Potential Zika Virus NS3$^{pro}$ Inhibitors

**Fernanda Kelly Marcelino e Oliveira [1], Beatriz Murta Rezende Moraes Ribeiro [2], Ellen Gonçalves de Oliveira [1], Marina Mol Sena Andrade Verzola [3], Thales Kronenberger [4,5], Vinícius Gonçalves Maltarollo [3], Ricardo José Alves [3], Renata Barbosa de Oliveira [3], Rafaela Salgado Ferreira [2], Jônatas Santos Abrahão [1] and Mateus Sá Magalhães Serafim [1,*]**

[1] Departament of Microbiology, Instituto de Ciências Biológicas, Universidade Federal de Minas Gerais (UFMG), Belo Horizonte 31270-901, Brazil
[2] Departament of Biochemistry and Immunology, Instituto de Ciências Biológicas, Universidade Federal de Minas Gerais (UFMG), Belo Horizonte 31270-901, Brazil
[3] Departament of Pharmaceutical Products, Faculdade de Farmácia, Universidade Federal de Minas Gerais (UFMG), Belo Horizonte 31270-901, Brazil
[4] Institut für Medizinische Mikrobiologie und Hygiene. Partner-site Tübingen, German Center for Infection Research (DZIF), Elfriede-Aulhorn-Str. 6, 72076 Tübingen, Germany; thales.kronenberger@uni-tuebingen.de
[5] School of Pharmacy, Faculty of Health Sciences, University of Eastern Finland, 70211 Kuopio, Finland
* Correspondence: mateusmserafim@gmail.com

**Abstract: Background/Objectives:** Zika fever is a disease caused by the Zika virus (ZIKV). Symptomatic cases may be associated with neurological disorders in adults, as well as congenital Zika syndrome and other birth defects during pregnancy. In 2016, Zika fever was considered a public health problem by the World Health Organization (WHO), highlighting the need to develop new therapies against the disease. Currently, there is no antiviral or vaccine available to treat or prevent severe cases. Due to the lack of available therapeutics and few promising hit molecules, we computationally screened the well-described ZIKV protease (NS3$^{pro}$) as a drug target to revisit the small-molecule database Brazilian Compound Library (BraCoLi) and select potential inhibitors. **Methods:** We employed a consensus docking screening of a library of 1176 compounds using GOLD and DockThor. We selected 28 hits based on predicted binding affinity, and only the remnants of three compounds were available in the library at the time of this study for experimental validation. The hits were evaluated for their cytotoxic ($CC_{50}$) and effective concentrations ($EC_{50}$) for their potential antiviral activity in Vero cells. **Results:** The three hit compounds presented modest $CC_{50}$ values of 89.15 ± 3.72, >100, and 29.67 ± 1.01 μM, with the latter, a carbohydrate derivative, having an $EC_{50}$ value of >12.5 μM (~40% inhibition) against ZIKV PE243. Additionally, the essentially non-toxic compound, an arylfuran derivative, also inhibited the ZIKV NS3$^{pro}$ with an $IC_{50}$ value of 17 μM but presented evidence of acting through a promiscuous mechanism for enzyme inhibition. **Conclusion:** This study highlights the relevance of revisiting existing small-molecule assets to identify novel therapeutic starting points against ZIKV, aiming for potential lead candidates in the future.

**Keywords:** antiviral activity; arylfuran derivative; consensus docking; MTT; NS3$^{pro}$; Zika virus



Academic Editor: Giuseppe Floresta

Received: 19 December 2024
Revised: 10 February 2025
Accepted: 13 February 2025
Published: 15 February 2025

**Citation:** Marcelino e Oliveira, F.K.; Murta Rezende Moraes Ribeiro, B.; Gonçalves de Oliveira, E.; Mol Sena Andrade Verzola, M.; Kronenberger, T.; Gonçalves Maltarollo, V.; Alves, R.J.; Barbosa de Oliveira, R.; Salgado Ferreira, R.; Santos Abrahão, J.; et al. Discovery of Arylfuran and Carbohydrate Derivatives from the BraCoLi Library as Potential Zika Virus NS3$^{pro}$ Inhibitors. *Future Pharmacol.* **2025**, *5*, 9. https://doi.org/10.3390/futurepharmacol5010009



## 1. Introduction

Zika fever is a disease caused by the Zika virus (ZIKV; *Orthoflavivirus zikaense* [1]) [2]. Similarly to dengue and yellow fever viruses, ZIKV is an arthropod-borne virus (i.e., arbovirus) from the genus *Flavivirus* [3] that infects the human host by the bite of mosquitoes

such as *Aedes aegypti* and *A. albopictus* [4,5]. This enveloped virus has a single-stranded and positive-sense RNA, which is translated into a single polyprotein that encodes three structural proteins, namely capsid (C), pre-membrane (prM), and envelope (E). In addition to these three, seven non-structural (NS) proteins (NS1, NS2A, NS2B, NS3, NS4A, NS4B, and NS5) are also released after the proteolytic processing, which helps in the viral replication, proteolysis, packaging of the genome, and viral assembly and release [6,7].

Aside from asymptomatic cases, ZIKV infections manifest in signs and symptoms such as headache, fever, and joint and muscle pain. Additionally, rash, skin itching, and redness in the eyes may occur [8]. Importantly, infections during pregnancy can lead to congenital Zika syndrome and birth defects [9]. For example, microcephaly is one of the most common associated cases, in which the newborn's head is smaller than expected as the brain stops developing after birth or is not developed properly during pregnancy [9–11]. Other neurological disorders or alterations have also been associated with Zika infection, such as the Guillain–Barré syndrome (GBS) in adults [12,13]. This syndrome is characterized as an autoimmune disease that can be caused by an infection (e.g., *Campylobacter jejuni* [14,15] and ZIKV [13]), in which an inflammation of the peripheral nerves occurs. This can cause partial or total paralysis of the patient, which can lead to death. Regarding the viral infection, it is hypothesized that the pathogenesis of this disease occurs with the production of neutralizing antibodies against ZIKV that act on nerve glycolipids, inducing an inflammatory response that causes lesions in the myelin or axonal membranes [13,16].

Currently, there are no vaccines available for ZIKV [17,18], and similar to dengue fever, Zika treatment relies on symptom relief [19]. In this context, no specific antiviral drugs have reached the market, despite various candidates being reported, such as nucleoside analogs, pyrimidine synthesis inhibitors, and even protease inhibitors [20,21]. Among the potential viral drug targets, the ZIKV protease, $NS3^{pro}$ [22], is broadly studied for the discovery of inhibitors [23–26], as it complexes with the cofactor NS2B (NS2B-NS3) and plays a fundamental role in the proteolysis of the viral polyprotein [6,22]. As traditional methods for screening bioactive compounds in vitro are time-consuming, computational simulations can be used to facilitate the design and discovery of potential antiviral drug candidates against ZIKV [27–31].

These computational approaches usually employ molecular docking as a starting point for compound (ligand) analysis or the screening of potential inhibitors against the target [32–35]. In our recent studies, we presented two different approaches for virtual screening (VS) campaigns considering thousands to millions of compounds [36,37]. New low-to-high micromolar hit compounds were identified from those strategies, such as aminopyrimidine derivatives [37], benzothiazoles [34], benzimidazoles [36], benzoic acid [38], and even the antibiotic novobiocin [39]. These combined various computational methods (e.g., docking) in a consensus approach, which are followed by in vitro experimental validation. Indeed, the combination of two or more different methods in a consensus approach can increase accuracy while focusing on one target or a broad-target approach. Aside from consensus VS, different docking simulations can also increase the robustness of a screening approach [40], which can improve the outcomes of individual compounds obtained from different software [41].

In the most recent study, the Brazilian Compound Library (BraCoLi) was accessed, despite yielding no hits from the consensus VS approach [37]. Herein, we proposed a consensus docking screening with two different free access software programs, GOLD 5.1 and DockThor version 2.0, after extensive software validation. These were used to screen 1176 compounds from BraCoLi as an attempt to revisit a small-molecule library in a faster approach for compounds' screening. We identified 16 potential $NS3^{pro}$ inhibitors, three

of which followed in vitro validation against ZIKV PE243 and enzyme inhibition assays. One carbohydrate derivative displayed antiviral activity in MTT assays, while an arylfuran derivative inhibited the $NS3^{pro}$ in the micromolar range. Taken together, this study demonstrates the feasibility of employing computational simulations and experimental validation when revisiting small libraries to search for potential novel $NS3^{pro}$ inhibitors.

## 2. Materials and Methods

### *2.1. Dataset, Ligands, and Target Preparation*

BraCoLi is a chemical library developed to facilitate the search for small-molecule chemical structures, having quick access to information on physicochemical and molecular properties. This 1176-compound collection comprises inhibitors that had been synthesized for over a decade between 2008 and 2018 to supply biological screenings to identify inhibitors with various activities, such as antiparasitic [42–44], antimicrobial [45–47], and antitumoral [48,49]. Arguably, this higher variety and consistency of data [50] could help in the search for new potential inhibitors. Ligands were prepared by building three-dimensional (3D) structural models using Discovery Studio. The lowest energy conformer of each compound was generated using an OMEGA 3.1.1.2 (OpenEye Scientific Software, USA, 2019); that is, the most stable conformational unit of a compound was generated among a maximum number of possible conformations. Next, the structures had their ionization state adjusted to pH 7.4 using FixpKa (QUACPAC 2.0.1.2, OpenEye Scientific Software, USA, 2019), which selected a single favorable ionization state. The ZIKV $NS3^{pro}$ (PDB ID: 5YOF [25], resolution of 1.51 Å) was selected due to the presence of a co-crystallized ligand in the complex and the absence of mutations. The target structure was prepared by removing water molecules, deleting double-occupancy data, and adding hydrogen atoms [51].

### *2.2. Binding Site Characterization*

The structure was submitted to the web servers FTSite and PrankWeb. FTSite predicts the interactions with these binding sites and residues, while PrankWeb predicts and ranks potential binding points on the protease surfaces by calculating the physicochemical and geometric properties of residues. Thus, residues that would be more relevant to a potential interaction were selected in a consensus from the two predictors. PyMOL software (v3.1.1 Schrödinger Inc., New York, NY, USA) was used to generate images.

### *2.3. Docking Standardization and Validation Using Redocking*

The intrinsic parameters of the programs were exhaustively standardized to better reproduce the experimental binding mode of the co-crystallized ligand and validate the systems [52]. The main parameters that can be modified in GOLD 5.1 [53] are fixing all protein rotatable bonds, configuration templates (i.e., default recommended settings for docking analysis), scoring function, number of genetic algorithm (GA) runs (i.e., iterations), and the distance of the atoms (in Å) defined from the protein binding site (i.e., size). As for DockThor, some of the parameters that can be changed are the binding site coordinates and grid size (up to 24 × 24 × 24 Å), as well as the search algorithm precision (standard or virtual screening), which essentially vary the number of runs (24 or 12) [54]. The root mean square deviation (RMSD) was used for comparison, and the parameters of each software that provided the lowest average RMSD values were selected to be used in the molecular docking analysis.

### *2.4. Consensus Molecular Docking Analysis*

The search parameters in GOLD 5.1 were (i) all protein rotatable bonds were fixed; (ii) the binding site defined with the co-crystallized ligand with all atoms within 6 Å; (iii) chemscore_kinase was the configuration template; (iv) 200 GA runs; (v) CHEMPLP was the scoring function, with no early termination allowed; and (vi) the GA search option was set as slow. The searching parameter in DockThor used was "Standard", and the grid box size was set at 20 × 20 × 20 Å, with a standard spacing of 1 Å between the grid points. Docking simulations with the 1176 compounds were performed using both software in subsets of up to 100 compounds to facilitate docking processing, and the results were compared by the overall highest GOLD scores (CHEMPLP fitness) and affinity (kcal/mol) calculated by DockThor [55] in a consensus scoring approach.

### *2.5. Similarity Calculations*

Similarity calculations between the screened compounds and molecules with anti-ZIKV activity were performed using a dataset retrieved from ChEMBL [56]. A subset of 608 compounds was obtained by searching "Zika virus" (ID: CHEMBL4296612), having 1028 associated bioactivities reported. Compounds having uncertainty measurements for their biological activities, non-inhibitors, and duplicates were removed from the analysis. The canonical SMILES of the screened compounds were used for the calculation of the Tanimoto coefficient (Tc) using RDkit nodes [57] (2024.09.5 documentation; available at https://www.rdkit.org, accessed on 23 November 2024) in KNIME [58]. Structural similarities were calculated using three different descriptors, namely Morgan, AtomPair, and MACCS fingerprints with default parameters.

### *2.6. Synthesis of BraCoLi Hit Compounds*

The analytical reagents used in the synthesis were obtained from commercial sources. Thin-layer chromatography (TLC) was performed using precoated 0.5 mm plates with a suspension formed by 8 g of silica gel 60 with $CaSO_4$ 13% *w*/*w* (Sigma Aldrich, Burlington, MA, USA) in 19 mL of distilled water. The melting points (mp) were determined on a Microquímica MQAPF 301 apparatus (Microquímica, Brazil). The NMR spectra were recorded on Bruker AVANCE DPX200 (200 MHz), Bruker AVANCE III HD NanoBay (400 MHz), or Bruker Avance Neo (600 MHz) spectrometers (Bruker, Billerica, MA, USA). Tetramethylsilane was used as an internal standard. Chemical shifts are expressed in a δ (ppm) scale, and J values are given in Hz, with the multiplicity of signals referred to as singlet (s), doublet (d), triplet (t), quartet (q), quintet (qt), double doublet (dd), double-double doublet (ddd), and multiplet (m).

### *2.7. Synthesis of 3-(5-(4-Bromophenyl)furan-2-carboxamido)propyl Methanesulfonate (**2**)*

In a round-bottom flask, 0.5 g (1.5 mmol) of amide 1 [59] solubilized in 30 mL of dichloromethane was added. Then, 660 µL (4.5 mmol) of triethylamine was added. The flask was immersed in an ice bath, and then 370 µL (4.5 mmol) of methanesulfonyl chloride was slowly added. The reaction mixture was kept under magnetic stirring at room temperature for 24 h when the consumption of the starting material was verified by TLC (eluent: ethyl acetate; stain: cerium ammonium molybdate solution 5% *w*/*v*). At the end of the reaction, the contents of the flask were transferred to a separatory funnel and washed with 20 mL of a 1.5 mol/L HCl solution. The aqueous phase was extracted with 20 mL of dichloromethane, and the combined organic phase was washed with saturated $NaHCO_3$ solution (2 × 20 mL) and then with distilled water (2 × 25 mL). The organic phase was then dried over $Na_2SO_4$, filtered, and evaporated in a rotary evaporator. The crude solid formed was purified by recrystallization in isopropanol, obtaining a yellow solid with a

41% yield. mp: 187–189 °C; $^{1}$H NMR (400 MHz, DMSO-*d*6): δ 7.96 (2H, d, *J* = 8.6 Hz), 7.75 (2H, d, *J* = 8.6 Hz), 7.74 (1H, d, *J* = 3.8 Hz), 7.43 (1H, d, *J* = 3.8 Hz), 4.76 (2H, t, *J* = 5.2 Hz), 3.66–3.68 (2H, m), 2.34 (3H, s), 2.22–2.27 (2H, m); $^{13}$C NMR (100 MHz, DMSO-*d*6): δ 157.9, 157.6, 139.4, 132.1, 127.2, 126.9, 123.4, 122.6, 109.7, 69.6, 38.2, 18.7.

### *2.8. Synthesis of N-(3-Azidopropyl)-5-(4-bromophenyl)furan-2-carboxamide (**3**)*

In a round-bottom flask containing 0.176 g (0.43 mmol) of the mesylated compound **2**, 2 mL of N,N-dimethylformamide (DMF) and 0.176 g (2.5 mmol) of sodium azide were added. The flask was coupled to a reflux condenser and closed with a $CaCl_2$ tube, and the reaction was maintained under magnetic stirring at 100 °C for approximately 24 h. At the end of the reaction, detected by TLC (eluent: ethyl acetate; stain: cerium ammonium molybdate solution 5% *w*/*v*), 20 mL of distilled water was added, and the contents of the flask were transferred to a separatory funnel. The aqueous phase was extracted with ethyl acetate (3 × 20 mL), and the organic phase obtained was washed with 25 mL of distilled water, dried with $Na_2SO_4$, filtered, and evaporated in a rotary evaporator. The residue obtained was then purified by silica column chromatography using hexane/ethyl acetate (8:2) as eluent, and the product, in the form of a light yellow solid, was obtained in 53% yield. mp: 45–47 °C; $^{1}$H NMR (400 MHz, DMSO-*d*6): δ 8.58 (1H, t, *J* = 5.3 Hz), 7.86 (2H, d, *J* = 8.4 Hz), 7.66 (2H, d, *J* = 8.4 Hz), 7.14 (1H, d, *J* = 3.3 Hz), 7.13 (1H, d, *J* = 3.3 Hz), 3.41 (2H, t, *J* = 6.7 Hz), 3.30–3.35 (2H, m), 1.78 (2H, qt, *J* = 6.7 Hz); $^{13}$C NMR (100 MHz, DMSO-*d*6): δ 157.6, 153.2, 147.3, 131.8, 128.6, 126.2, 121.6, 115.4, 108.2, 48.5, 35.9, 25.6.

### *2.9. Synthesis of 5-(4-Bromophenyl)-N-(3-(4-phenyl-1H-1,2,3-triazol-1-yl)propyl)furan-2-carboxamide (**BR020113**)*

In a round-bottom flask, 0.05 g (0.14 mmol) of azide derivative **3** and 16.4 µL (0.015 g; 0.14 mmol) of phenylacetylene, solubilized in 2 mL of THF, were added. Then, 0.023 g (0.11 mmol) of sodium ascorbate and 95.7 µL (0.05 mmol) of 10% aqueous $CuSO_4.5H_2O$ solution were added. The reaction mixture was kept under magnetic stirring at room temperature for approximately 3 h, when the consumption of the starting materials and formation of the product were detected by TLC (eluent: hexane/ethyl acetate 7:3; stain: iodine vapor). At the end of the reaction, ethanol was added to the flask and the precipitate formed was filtered and washed with methanol. The filtrate was evaporated on a rotary evaporator. The residue obtained was purified by silica column chromatography using hexane/ethyl acetate (1:1) as the eluent, and the product, in the form of a beige solid, was obtained with a 46% yield. mp: 161.9–162.6 °C; $^{1}$H NMR (400 MHz, DMSO-*d*6): δ 8.63 (1H, t, *J* = 3.5 Hz), 8.60 (1H, s), 7.85 (2H, d, *J* = 8.5 Hz), 7.81–7.84 (2H, m), 7.66 (2H, d, *J* = 8.5 Hz), 7.43 (2H, t, *J* = 7.6 Hz), 7.30–7.33 (1H, m), 7.16 (1H, d, *J* = 3.5 Hz), 7.13 (1H, d, *J* = 3.5 Hz), 4.48 (2H, t, *J* = 6.9 Hz), 3.33–3.36 (2H, m), 2.16 (2H, q, *J* = 6.9 Hz); $^{13}$C NMR (100 MHz, DMSO-*d*6): δ 157.7, 153.2, 147.3, 146.2, 131.84, 130.9, 128.8, 128.6, 127.7, 126.2, 125.0, 121.6, 121.4, 115.5, 108.3, 47.5, 35.9, 29.9; HRMS (*m*/*z*) 451.0765; 453.0747 (isotopes, $^{79}$Br and $^{81}$Br) $[M+H]^+$ calculated for $C_{22}H_{20}BrN_4O_2^+$: 451.0764; 453.0744.

### *2.10. Synthesis of Methyl 2,3-Di-O-benzyl-6-deoxy-6-[(2-iodobenzoyl)amino]-α-D-glucopyranoside (**5**)*

In a round-bottom flask containing 1.0 g (3.75 mmol) of 2-iodobenzoyl chloride and 10 mL of anhydrous acetone, a mixture of 0.55 g (1.5 mmol) of amino derivative **4** in 15 mL of acetone and 10 mL of saturated sodium carbonate solution was added under ice bath and magnetic stirring. The reaction mixture was kept under magnetic stirring at room temperature for 15 h. After removal of the acetone, 50 mL of distilled water was added, and the mixture was transferred to a separatory funnel and washed with dichloromethane (3 × 40 mL). The combined organic phase was dried over $Na_2SO_4$, filtered, and evaporated

in a rotary evaporator. The solid obtained was recrystallized with an ethanol/water mixture, obtaining amide **5** with a 79% yield. mp: 148.6–149.9 °C; $^{1}$H NMR (200 MHz, CDCl3): δ 7.84 (1H, d, *J* = 8.2 Hz), 7.40–7.24 (12H, m), 7.08 (1H, ddd, *J* = 8.2, 6.3, 2.9 Hz), 6.21 (1H, s), 4.89–4.87 (2H, m), 4.78 (1H, d, *J* = 12.1 Hz), 4.62 (1H, d, *J* = 12.1 Hz), 4.51 (1H, d, *J* = 3.6 Hz), 4.15–4.00 (1H, m), 3.84 (1H, t, *J* = 9.0 Hz), 3.74–3.52 (2H, m), 3.46–3.35 (1H, m), 3.42 (1H, dd, *J* = 9.0, 3.6 Hz), 3.36 (3H, s); $^{13}$C NMR (50 MHz, $CDCl_3$): δ 170.6, 141.4–127.6, 98.57, 92.4, 80.8, 79.3, 75.5, 73.4, 71.3, 70.1, 55.4, 40.5.

### *2.11. Synthesis of Methyl 2,3-Di-O-benzyl-4-O-cinnamoyl-6-deoxy-6-[(2-iodobenzoyl)amino]-α-D-glucopyranoside (***BR020325***)*

In a round-bottom flask containing 0.22 g (1.35 mmol) of cinnamoyl chloride and 5 mL of anhydrous acetone, a mixture of 0.35 g (0.58 mmol) of amide **5** in 10 mL of pyridine was added under ice bath and magnetic stirring. The reaction mixture was kept under magnetic stirring at room temperature for 17 h. The reaction mixture was poured into a beaker containing crushed ice, and 37% hydrochloric acid was added dropwise until pH 1 was reached. A brown precipitate formed and was filtered and then dissolved in dichloromethane, transferred to a separatory funnel, and washed with 10% sodium bicarbonate solution (2 × 50 mL) and distilled water (1 × 50 mL). The organic phase was dried over $Na_2SO_4$, filtered, and evaporated in a rotary evaporator. The residue obtained was purified by silica column chromatography using hexane/ethyl acetate (9:1, 8:2, and 7:3) as eluent, and the product, in the form of a beige solid, was obtained with a 29% yield. mp: 179.5–180.9 °C; $^{1}$H NMR (600 MHz, $CDCl_3$): 7.68 (1H, d, *J* = 7.8 Hz), 7.56 (1H, d, *J* = 15.6 Hz, H-8), 7.40–7.37 (2H, m), 7.29–7.09 (13H, m), 7.06 (1H, t, *J* = 7.8 Hz), 6.91 (1H, dt, *J* = 7.8 Hz; *J* = 1.2 Hz), 6.27–6.24 (1H, m), 6.22 (1H, d, *J* = 15.6 Hz), 4.93 (1H, t, *J* = 9.6 Hz), 4.76 (1H, d, *J* = 11.4 Hz), 4.69 (1H, d, *J* = 12.6 Hz), 4.59 (1H, d, *J* = 11.4 Hz), 4.55 (1H, d, *J* = 12.6 Hz), 4.50 (1H, d, *J* = 3.6 Hz, H-1), 3.94 (1H, t, *J* = 9.6 Hz), 3.86–3.81 (2H, m), 3.48 (1H, dd, *J* = 9.6, 3.6), 3.31 (3H, s), 3.16–3.11 (1H, m); $^{13}$C NMR (50 MHz, $CDCl_3$): δ 169.2, 166.3, 146.1, 142.1–127.5, 117.0, 98.2, 92.3, 79.5, 78.6, 75.5, 73.5, 71.3, 68.0, 55.7, 39.8.

### *2.12. Cell Lineage and Virus*

Vero cells (ATCC® CCL-81™) and African green monkey kidney epithelial cells (fibroblasts) were used for cell assays. Cells were cultured in minimum essential medium (MEM) supplemented with 5% fetal bovine serum (FBS), 100 IU/mL of penicillin (Cellofarm, Brazil), 100 µg/mL of streptomycin (Merck, Germany), and 0.25 µg/mL amphotericin B (Cultilab, Brazil). Incubations were performed in a humidified incubator at 37 °C and a 5% $CO_2$ atmosphere. ZIKV (PE243) was kindly provided by the Laboratório de Vírus at Universidade Federal de Minas Gerais (UFMG). The virus was isolated in Recife, Pernambuco, Brazil, in 2015 at the Oswaldo Cruz Foundation (FIOCRUZ), as described [60]. This study is registered in the National System for the Management of Genetic Heritage and Associated Traditional Knowledge (SisGen), code A7AF7BF.

### *2.13. Viral Propagation and Titration*

Viral stocks were prepared as described [61]. Briefly, ZIKV propagation was performed in Vero cells. Cells in 12 mL of MEM 5% FBS were seeded in T-75 culture flasks and incubated under the same conditions above. After 24 h of incubation, cell monolayers (~60% confluency) were washed with PBS for the removal of cell debris and FBS. Cells were infected with ZIKV (PE243) in 2.0 mL of serum-free MEM at a multiplicity of infection (MOI) of 0.01, i.e., one viral particle for every 100 cells in culture (1:100). Adsorption was performed for 1 h at 37 °C and 5% $CO_2$, delicately homogenizing the flasks, that is, slowly swaying vertically and horizontally (cross shape) every 10 min to facilitate the adsorption of viral particles in the cells. Then, 12 mL of MEM 2% FBS was added to the

flasks and incubated. The occurrence of cytopathic effects (CPEs) was monitored daily, and by evidencing effects in ~70 to 80% of the cells, the supernatant was removed and centrifuged at 2016× *g* and 4 °C for 10 min for the removal of cellular debris. Supernatants were aliquoted into 1.5 mL microtubes and stored at −70 °C for titration.

Titration was performed to determine the concentration of viral particles in stock samples. Here, cells in 1.0 mL of MEM 1% FBS were seeded in 24-well microplates (80,000 cells per well) and incubated. Then, slowly thawed (ice bath) ZIKV stock samples were diluted in 100 µL of serum-free MEM in a 1:10 ratio ($10^{-1}$ to $10^{-5}$) and added in triplicate to the microplate. Wells with no added viral samples were used as negative controls. Adsorption was performed for 1 h as above, and 2.0 mL of 199 media supplemented with 1% carboxymethylcellulose (CMC) and 2% FBS were added per well and incubated for five days. After incubation, each well's content was fixed with 3.7% *v*/*v* formaldehyde for 24 h, washed carefully (wall of the well) with water using a laboratory wash bottle, and stained with violet crystal for 20 min. Finally, the microplates were washed again, and the plaque-forming units (PFU) in each well were counted (naked eye) to calculate the concentration of viral particles per milliliter (PFU/mL).

### *2.14. MTT Assays on Cytotoxicity and Antiviral Activity*

The concentration of the tested compounds at which the viability of Vero cells was reduced by 50%, that is, the cytotoxic concentration of 50% ($CC_{50}$), was assessed using the MTT (3-(4,5-dimethylthiazol-2-yl)-2,5-diphenyltetrazolium bromide; Thermo Fisher Scientific, Waltham, MA, USA) assay [62]. MTT assays were performed as reported [61]. Briefly, cells in 100 µL of MEM 1% FBS were seeded in 96-well microplates (40,000 cells per well) and incubated. After 24 h, media were removed, and 100 µL of compounds in MEM 1% was added over seven concentrations (100 to 1.56 µM) in triplicate and incubated. After 72 h of incubation, the media were removed, and 100 µL of MTT in MEM 1% FBS (0.5 mg/mL) was added to each well and incubated. After 3 h, the media were removed, and 100 µL of DMSO was added to solubilize the formazan crystals. The wells' content was homogenized by shaking the microplates using a magnetic stirrer for 20 min, and readings were performed using a spectrophotometer (VersaMax, San Jose, CA, USA) at a wavelength of 570 nm. Linear regression was used to calculate $CC_{50}$ values in Microsoft Excel, considering $R^2 > 0.85$. The percentage of inhibition was normalized with DMSO controls (0.5 to 0.0156% *v*/*v*) and compared to cells without compounds or DMSO. An inhibition control (DMSO 10% *v*/*v*) was also added. One independent assay in quadruplicate was performed ($n$ = 4 data points).

Antiviral activity was also assessed using the MTT assays as reported [61,63]. Briefly, the same conditions were followed as above. Viral suspensions at a MOI of 0.1 in 100 µL of serum-free MEM were added to each well in triplicate 1 h before adding the serial dilution of compounds (below the $CC_{50}$ values). The microplate was incubated for 72 h as above. The effective concentration at which cytopathic effects were decreased by 50%, that is, the effective concentration of 50% ($EC_{50}$), was calculated relative to the DMSO controls (infected cells in MEM containing DMSO). Ribavirin, the hepatitis C drug, was used as an inhibition control. Selectivity index (SI) values were calculated as $CC_{50}/EC_{50}$. One independent assay in quadruplicate was performed ($n$ = 4 data points).

### *2.15. Expression and Purification of Recombinant ZIKV NS2B-NS3$^{pro}$*

The ZIKV NS2B-NS3$^{pro}$ was expressed and purified using the construct as described previously [36]. This construct comprises the viral protease from the Brazilian isolate BeH823339, linked by a Gly4-Ser-Gly4 sequence between the two protein domains. There are four incorporated substitutions, namely R96A (NS2B) and R29G/C80S/C143S (NS3),

all within a pET-15b plasmid (SisGen code: ACCD10D). Briefly, *Escherichia coli* BL21-DE3 cells, which contained the ZIKV NS2B-NS3$^{pro}$ construct, were incubated overnight at 37 °C and 200 rpm in 12.5 mL of 2xYT medium supplemented with 100 µg/mL of ampicillin. After incubation, the culture was added to 1 L of fresh media and incubated under the same conditions until reaching an optical density (OD) of 0.7 ± 0.1. To induce overexpression, 1 mM isopropyl-β-D-galactoside (IPTG) was added to the culture and incubated overnight at 20 °C and 200 rpm. After incubation, the culture was centrifuged for 30 min at 4 °C and 5000 rpm and resuspended in 20 mL of buffer "A" consisting of 25 mM Tris-HCl at pH 8.5, 10 mM NaCl, and 5% glycerol. Last, cells were lysed by sonication (20/40 s on/off pulses) while maintained on ice, followed by centrifugation at 10,000 × *g* for 1 h at 4 °C.

The culture supernatant was loaded into a 5 mL HisTrap Sepharose HP nickel column (GE Healthcare, USA) and eluted with a flow rate of 1 mL/min using a linear gradient (0 to 100%) of buffer "B" (25 mM Tris-HCl at pH 8.5, 500 mM NaCl, 500 mM imidazole, and 5% glycerol) spanning five column volumes. The protein solution was then transferred to a HiLoad 16/600 Superdex 75pg gel filtration column (GE Healthcare, Chicago, IL, USA) and eluted with buffer "A" at a flow rate of 0.1 mL/min, spanning 1.2 column volumes. Lastly, the purified protein samples were stored at −80 °C.

### *2.16. Enzymatic Inhibition Assays*

The activity of recombinant ZIKV NS2B-NS3$^{pro}$ was measured by monitoring the fluorescence signal generated from the cleavage of the fluorogenic substrate Bz-Nle-Lys-Lys-Arg-AMC using a Biotek Synergy 2 microplate reader (excitation λ: 340 nm; emission λ: 440 nm). Readings were recorded continuously for at least 2 min. All assays were performed as previously reported [36,64] in a buffer containing 10 mM Tris-HCl at pH 8.5, 0.005% Tween 20, and 5% glycerol, with a final concentration of 9 nM enzyme and 44 µM substrate. All assays were performed in triplicate in two independent assays, with results reported as mean values with standard deviations ($n$ = 6 data points).

For the initial screening, each compound was tested at 100 µM after a 10 min pre-incubation with the enzyme at 37 °C, followed by adding the substrate. Compounds showing at least 50% inhibition were further analyzed without pre-incubation. $IC_{50}$ values were determined by evaluating at least six concentrations (0–200 µM) and calculated using GraphPad Prism 6.0 by fitting to the four-parameter $IC_{50}$ Equation (1) as follows:

$$Y = Bottom + [Top - Bottom/1 + 10^{(logIC_{50} - X) \times s}], \quad (1)$$

where "X" is the inhibitor concentration, "s" is the slope of the concentration–response curve (Hill slope), and the top and the bottom are, respectively, the upper and bottom plateaus. Sensitivity to detergent was assessed by replacing Tween 20 with Triton X-100 in the assay buffer. Three different concentrations of Triton X-100 were evaluated (0.001%, 0.01%, and 0.01%). Sensitivity to BSA was assessed using a buffer containing 0.001% Triton X-100. In this assay, compounds at concentrations near their $IC_{50}$ were pre-incubated with 4 mg/mL of BSA (resulting in a final concentration of 1 mg/mL in the assay) for 10 min. Afterwards, the enzyme was added, followed by an additional 10 min incubation before adding the substrate, and readings were performed as above.

## 3. Results

### *3.1. Computational Simulations with ZIKV NS3$^{pro}$*

#### 3.1.1. Extensive Docking Standardization Validated Both Docking Software

Initially, redocking with the ZIKV NS3$^{pro}$ (PDB ID: 5YOF) was performed to assess the ability of each software program to reproduce the experimental binding mode of

the co-crystallized ligand (7HS, a positively charged dipeptide inhibitor: Lys-Arg) while varying each docking parameter [51,52]. Thus, we selected the lowest RMSD value (Å) poses and their corresponding docking scores for comparison purposes. As for the GOLD software, we combined configuration templates (recommended settings for docking), scoring functions, number of runs (iterations), and binding site size (Å). First, we combined three different available configuration templates (chemscore_kinase, gold_kinase, and gold_serine_protease) and scoring functions (CHEMPLP, ChemScore, and GoldScore) by using "fix all protein rotatable bonds", a minimum binding site size (6 Å), and a maximum number of genetic algorithm (GA) runs ($n$ = 200). Comparing the configuration templates (Table 1), "chemscore_kinase" had an overall similar range of RMSD values (0.88 to 1.19 Å) to "gold_kinase" (0.89 to 1.15 Å), which were slightly lower than "gold_serine_protease" (1.06 to 1.23 Å). The first two were consistent with both the "CHEMPLP" and "ChemScore" scoring functions having lower RMSD values compared to "GoldScore".

**Table 1.** Redocking 7HS using GOLD.

| Configuration Template [1] | Scoring Function | Lowest RMSD (Å) | Docking Score |
|---|---|---|---|
| chemscore_kinase | CHEMPLP | 1.01 | 72.82 |
| chemscore_kinase | ChemScore | 0.88 | 16.71 |
| chemscore_kinase | GoldScore | 1.19 | 63.12 |
| gold_kinase | CHEMPLP | 0.89 | 71.44 |
| gold_kinase | ChemScore | 0.95 | 19.53 |
| gold_kinase | GoldScore | 1.15 | 60.36 |
| gold_serine_protease | CHEMPLP | 1.23 | 65.28 |
| gold_serine_protease | ChemScore | 1.12 | 16.47 |
| gold_serine_protease | GoldScore | 1.06 | 57.56 |

[1] Available docking configuration templates with recommended settings in GOLD 5.1.

Furthermore, aiming to assess if the fitting of potential inhibitors would not be impaired by smaller sites or if a potential loss of selectivity could occur in larger sites, we varied the target site sizes. Default sizes of 6, 10, and 20 Å were selected using the "chemscore_kinase" template. Herein, 6 Å had the lowest average (top three) RMSD values (1.15 Å) compared to 10 (1.39 Å) and 20 Å (1.30 Å) sites (Table S1). Also, aiming to understand if the maximum number of GA runs would be necessary for higher accuracy in the consensus screening, we varied the number of GA runs (10, 20, 100, and 200) with CHEMPLP and ChemScore using the "chemscore_kinase" template. The results demonstrate the overall lower average (top three) RMSD results for CHEMPLP (2.15 Å) than ChemScore (4.91 Å) employing 10 GA runs only, while similar results were obtained for 20, 100, and 200 runs, respectively (1.62, 1.65, and 1.11 vs. 1.56, 1.03, and 0.94 Å). As expected, a higher number of GA runs maintained the lower overall RMSD values due to the increasing probability of achieving a more reproducible redocking pose. Therefore, considering the slight difference for 200 GA runs but a notable difference for 10 GA runs, we reaffirmed the use of 6 Å and 200 GA runs with the "chemscore_kinase" template and CHEMPLP scoring function. The latter is the default in GOLD 5.1 [53,65] as an optimized scoring function for pose prediction [65–67]. All combinations used in the redocking simulations are available on Table S1.

Additionally, we also assessed the combination of available parameters in DockThor, such as grid size (10 × 10 × 10 or 20 × 20 × 20 Å) and search algorithm precision (standard or virtual screening). Similarly to the GOLD results, the default parameters in DockThor, 20 × 20 × 20 Å, and the standard algorithm provided slightly lower RMSD values and equivalent affinity scores compared to the virtual screening parameters (Table 2). Taken

together, the two redocking analyses support the use of both software default parameters in the following consensus docking approach.

**Table 2.** Redocking 7HS using DockThor.

| Grid Size (Å) | Algorithm Precision | RMSD (Å) | Affinity (kcal/mol) |
|---|---|---|---|
| 20 | Standard | 1.76 | −7.54 |
| 20 | Virtual Screening | 1.78 | −7.54 |
| 10 | Standard | 28.08 | −5.63 |
| 10 | Virtual Screening | 2.19 | −6.91 |

### 3.1.2. Characterization of ZIKV NS3$^{pro}$ Predicted Important Residues for Interaction

To understand the target selectivity of the potential ZIKV NS3$^{pro}$ inhibitors, we focused on characterizing the residues that would potentially interact with the screened ligands. Characterization of the potential binding sites was conducted using FTSite, which predicted three different sites (blue, green, and red meshes). The first and larger (blue) encompasses 14, including Asp83 and Phe84 (NS2B, in orange), His51, Tyr130, Pro131, Ala132, Thr134, Ser135, Tyr150, Gly151, Asn152, Gly153, Val155, and Tyr161 (Figure 1A). PrankWeb ranked two potential binding sites, the first predicted to have a score of 10.57 and a probability of 60.7%, and the second having a lower score (2.42) and probability (6.5%). The results from the most probable predicted site (Figure 1B) had the same residues as FTSite, with the addition of a smaller hydrophobic region composed of Trp50 and Val72. In addition, Ser81 and Gly82 (NS2B), Lys54, Val72, Asp75, and Asp129 were predicted only by PrankWeb (labeled in black), while Phe84 (NS2B) was only predicted by the FTSite (labeled in black). These results support a common binding site being predicted by different software, which could indicate a conserved region for potential inhibitors to interact with the NS3$^{pro}$. In support of this notion, the co-crystallized ligand 7HS also occupies this predicted region (Figure 1C).

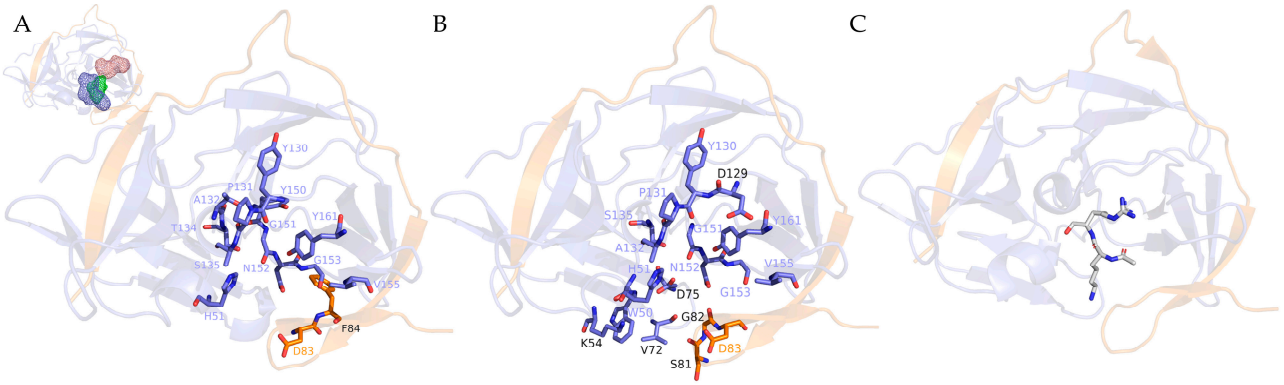


**Figure 1.** Characterization of the ZIKV NS3$^{pro}$ binding site. (**A**) FTsite predictions of the NS3$^{pro}$ (slate) and the NS2B* cofactor (orange) predicted three binding sites (blue, green, and red meshes), with the larger binding site highlighting residues in sticks as follows: Asp83 and Phe84 (NS2B), His51, Tyr130, Pro131, Ala132 Thr134, Ser135, Tyr150, Gly151, Asn152, Gly153, Val155, and Tyr161. (**B**) PrankWeb predictions corroborate FTSite with additional residues, such as Ser81 and Gly82 (NS2B), Lys54, Val72, Asp75, and Asp129. Lastly, (**C**) the co-crystallized ligand 7HS (white) also occupies the predicted binding site region. Predicted residues are shown as sticks and labeled. Unique residues predicted by each software are labeled in black. Images were generated with PyMOL (v.2.5.7).

### 3.1.3. Consensus Screening of BraCoLi Ligands Resulted in 16 Potential NS3$^{pro}$ Inhibitors

The 1176 compounds, divided into subsets of 100 compounds, were submitted to GOLD and DockThor considering the parameters defined in our redocking validation. The

top five structures with the highest scores, that is, higher CHEMPLP fitness and lower affinity (kcal/mol) scores from each of the 12 subsets were selected in a consensus scoring approach [55], resulting in 60 compounds from each docking simulation (Table S2). Then, we selected only those that were predicted to have the highest scores from both docking simulations (Tables 1 and 2), that is, fitness > 72.82 and affinity < −7.54, so that each software program was complementary to the other. Thus, a total of 28 compounds (Table S2) were selected for the assays. **BR010385** was predicted to have the highest CHEMPLP fitness (110.2) and affinity (−10.1) scores, closely followed by its structural analog, **BR010384** (106.9 and −8.92, respectively). A visual inspection of the GOLD docking pose of **BR010385** (Figure S1A) showed predicted interactions via hydrogen bonds with important ZIKV $NS3^{pro}$ residues [37], such as Asp129, Gly153, Val155, and Tyr161, as well as Ser81 and Asp83 (NS2B), which are consistent with our binding site characterization results (Figure 1). A similar docking pose was observed for **384** (Figure S1B), despite only Asp129 and Tyr161 being predicted to interact with this ligand via hydrogen bonds.

At the time of this study, however, among the 28 hits, only the remnants of three compounds were available in the library for experimental validation, comprising **BR020113**, **BR020255**, and **BR020325**. For instance, **BR020113** was predicted to have only one interaction via a hydrogen bond with Asn152 (Figure 2A), while **BR020255** was predicted to interact with Lys54 and Tyr161 (Figure 2B). Lastly, **BR020325**, which showed the highest scores among these three compounds (82.7 and −9.11), was predicted to interact with Tyr130, Ser135, Gly153, and Tyr161 (Figure 2C). An important interaction with the catalytic serine (nucleophile) was predicted from the ligand phenol ring with the hydroxyl of Ser135 (distance of 1.6 Å), while the ether stabilizes the interaction with the carboxyl of Gly151. This interaction with Ser135 is desirable for potential inhibitors, as this catalytic residue triggers enzyme proteolytic activity [68].

The arylfuran derivative **BR020255** was synthesized as described previously [69]. The other arylfuran derivative, **BR020113**, was synthesized in three steps from 5-(4-bromophenyl)-N-(3-hydroxypropyl)furan-2-carboxamide **1** [59], as shown in Scheme 1 (Figure 3A). A carbohydrate derivative, the amidoester **BR020325**, was obtained in two steps from amino derivative **4** [70], with the formation of amide **5** using 2-iodobenzoyl chloride, followed by esterification of the free hydroxyl at C-5 by reaction with cinnamoyl chloride, as shown in Scheme 2 (Figure 3B). The $^{1}H$ and $^{13}C$ nuclear magnetic resonance (NMR) spectra of the two newly described compounds, **BR020113** and **BR020325**, are available in Figures S3–S8.

#### 3.1.4. Structural Similarities are Predicted for BR020113, BR020255, and BR020325 and Known Anti-ZIKV Compounds

Finally, we compared the three selected structures with anti-ZIKV compounds from ChEMBL using three different fingerprints. These calculations suggested that our hits are structurally different (Tanimoto coefficient < 0.62) from active compounds reported in the literature (Figure 4). The similarity values from this ChEMBL subset, based on Tc calculations, ranged from 0.98% to 61.29%. The higher similarity corresponds to the compound that shares most similarities with **BR020113** (ID: CHEMBL4871785) using MACCS. This fingerprint (166 bits) is much simpler in comparison with Morgan and AtomPair (1024 bits). Also, MACCS calculated the highest similarity with **BR020255** (ID: CHEMBL379110; 58.97%) and **BR020325** (ID: CHEMBL4636584; 56.45%). The ChEMBL compounds have shown different activities (e.g., cell-based, $EC_{50}$, and enzymatic, $IC_{50}$) in the micromolar range against ZIKV, which could indicate our hits to be active against ZIKV PE243.

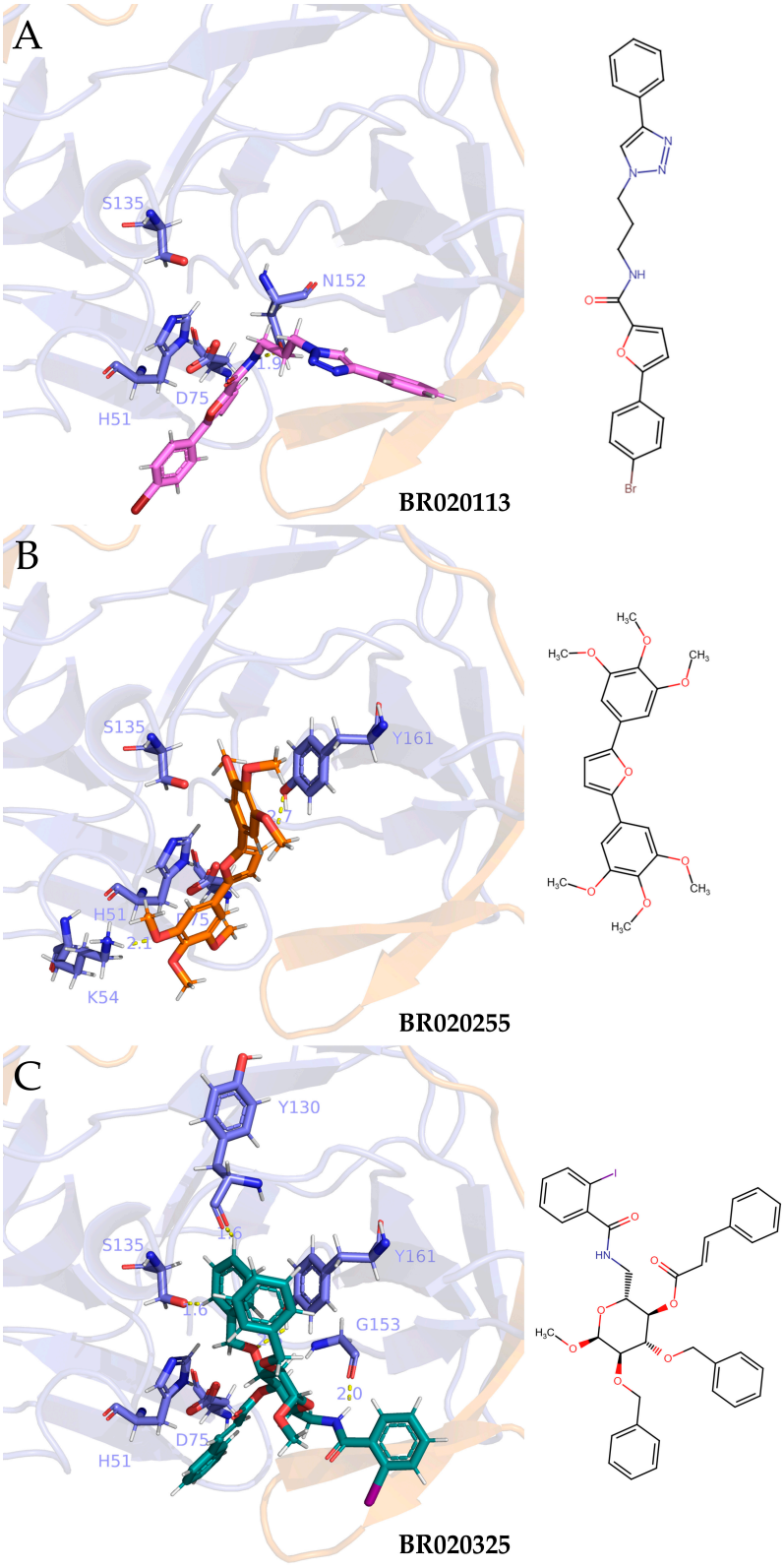


**Figure 2.** Docking poses of **BR020113**, **BR020255**, and **BR020325** to the ZIKV NS3$^{pro}$. (**A**) **BR020113** (violet) was predicted to have only one interaction with Asn152 and (**B**) **BR020255** (orange) was predicted to interact with Lys54 and Tyr161 despite not accurately fitting the binding site. Lastly, (**C**) **BR020325** (deep teal) interacted with Tyr130, Ser135, Gly153, and Tyr161. The ZIKV NS3$^{pro}$ (slate) and the cofactor NS2B (orange) are shown as a transparent cartoon. Residues are shown as sticks and labeled. Predicted interactions are shown as dashed yellow lines. Images were generated with PyMOL (v.2.5.7).

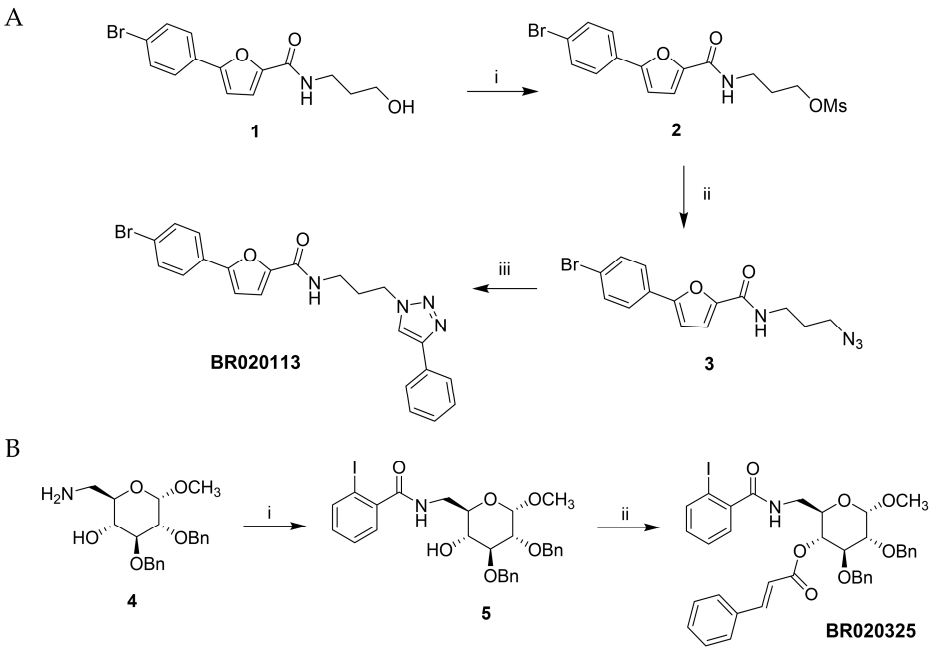


**Figure 3.** Synthesis routes to obtain compounds **BR020113** and **BR020325**. (**A**) Scheme 1 (**BR020113**) conditions and reagents: (i) $CH_3SO_2Cl$, $CH_2Cl_2$, $Et_3N$ (yield: 41%); (ii) $NaN_3$, DMF, 100 °C (yield: 53%); (iii) phenylacetylene, $CuSO_4.5H_2O$, sodium ascorbate, THF (yield: 46%). (**B**) Scheme 2 (**BR020325**) conditions and reagents: (i) 2-iodobenzoyl chloride, saturated $Na_2CO_3$ solution, anhydrous acetone (yield: 79%); (ii) cinnamoyl chloride, pyridine, anhydrous acetone (yield: 29%).

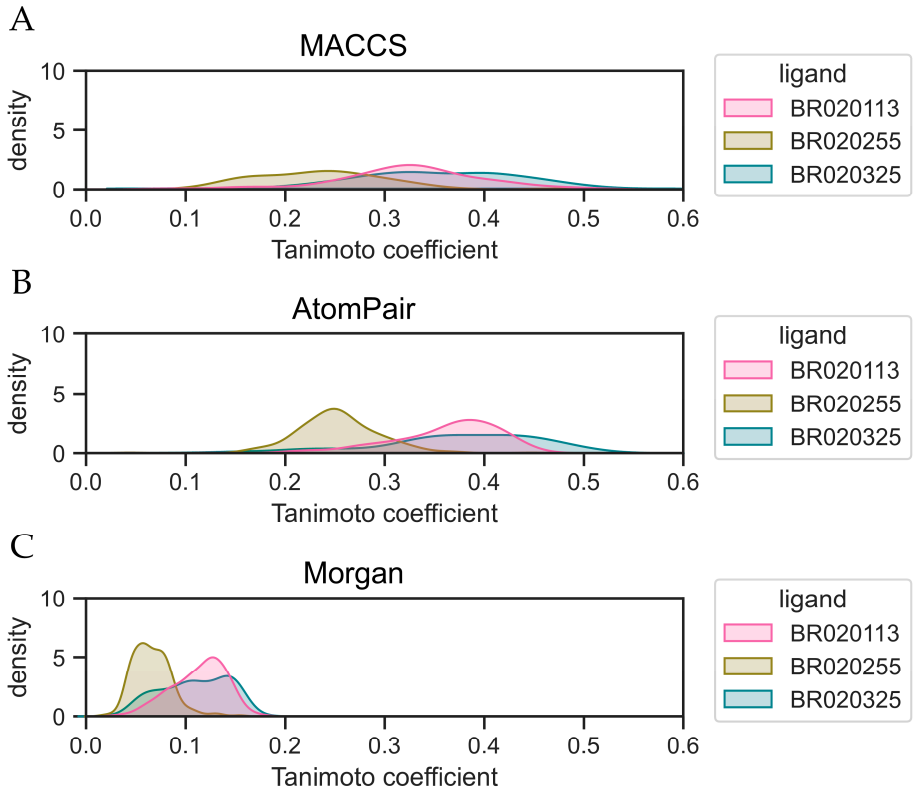


**Figure 4.** Structural similarity (Tanimoto coefficient; Tc) of **BR020113**, **BR020255**, and **BR020325** with anti-ZIKV compounds. Active compounds against ZIKV were retrieved from ChEMBL and compared to the three hits using (**A**) MACCS (166 bits), (**B**) AtomPair (1024 bits), and (**C**) Morgan (1024 bits) fingerprints.

### *3.2. Experimental Validation with ZIKV PE243 and ZIKV NS3$^{pro}$*

#### 3.2.1. MTT Assays Demonstrate BR020325 Antiviral Activity Against ZIKV

We followed the experimental validation of the three compounds by determining their cytotoxicity and antiviral activity in Vero cells using MTT assays (Table 3). Compound **BR020113** had a $CC_{50}$ value of 89.15 ± 3.72 μM, while the $CC_{50}$ value of **BR020255** was >100 μM. Conversely, **BR020325** had the lowest $CC_{50}$ value of 29.67 ± 1.01 μM. The three compounds were tested below their $CC_{50}$ values, at 50, 100, and 12.5 μM, respectively. Only compound **BR020325** showed antiviral activity against ZIKV PE243, by inhibiting 40.13% of viral cytopathic effects at 12.5 μM, essentially an $EC_{50}$ > 12.5 μM and SI < 2.37. Thus, one could suggest that **BR020325** antiviral activity could be associated with the proposed target inhibition.

**Table 3.** Evaluation of the cytotoxicity and antiviral activity of **BR020113**, **BR020255**, and **BR020325**.

| Compound | $CC_{50}$ (μM) | $EC_{50}$ (μM) | SI [1] ($CC_{50}/EC_{50}$) |
|---|---|---|---|
| **BR020113** | 89.15 ± 3.72 | - | - |
| **BR020255** | >100 | - | - |
| **BR020325** | 29.67 ± 1.01 | >12.5 μM (40.13%) [2] | <2.37 |
| Ribavirin [3] | >100 | 4.1 ± 0.35 | >24.39 |

[1] Selectivity index: ratio between $CC_{50}$ and $EC_{50}$ values. Reported values are represented as the average and standard deviation calculated from one independent assay in quadruplicate ($n$ = 4 data points). [2] Compound **BR020325** inhibited 40.13% of ZIKV cytopathic effects at 12.5 μM. [3] Ribavirin data were reported by us previously [61].

#### 3.2.2. Enzymatic Inhibition Assays Identify BR020255 as a ZIKV NS3$^{pro}$ Inhibitor

We next evaluated the ZIKV NS3$^{pro}$ inhibition assays to validate the three compounds. Initially, the compounds were assessed at 100 μM with a 10 min pre-incubation with the enzyme. Only **BR020255** presented over 50% inhibition at this condition, and no inhibitory effect was observed for this compound in the assays without pre-incubation, thus indicating a time-dependent inhibition. The $IC_{50}$ value of **BR020255** was determined to be ~17 μM (Table 4), but it exhibited a high Hill coefficient of ~5.9 (Figure S2), indicating positive cooperativity, which may be associated with an aggregating behavior of the inhibitor [71].

**Table 4.** Percentages of ZIKV NS2B-NS3$^{pro}$ activity inhibition and half-maximum inhibitory concentration ($IC_{50}$) values (μM) for each compound.

| | % Inhibition at 100 μM [1] | | $IC_{50}$ (μM) |
|---|---|---|---|
| Compound | With Incubation | Without Incubation | |
| **BR020113** | 7 ± 3 | ND | ND |
| **BR020255** | 100 | 0 | 16.995 ± 0.0636 |
| **BR020325** | 6 ± 3 | ND | ND |

[1] Assays were performed in 10 mM Tris-HCl, 5% $v/v$ glycerin, and 0.005% Tween 20 at pH 8.5, in the presence of 9 nM enzyme and 44 μM substrate at 37 °C. Reported values are represented as the average and standard deviation calculated from two independent assays in triplicate ($n$ = 6 data points). ND: not determined.

To further explore the possibility that the compound inhibits the enzyme through colloidal aggregation, two assays were conducted, both replacing the detergent Tween 20 with Triton X-100 (Table 5). In the first assay, enzymatic activity was evaluated under three buffer conditions containing 0.001%, 0.01%, and 0.1% Triton X-100. The compound exhibited low inhibition when tested at a concentration of 20 μM, which is close to its determined $IC_{50}$. At this concentration, no significant changes in inhibition were observed in either BSA or a Triton X-100 assay. Conversely, at 50 μM, a decrease in inhibition was observed when the concentration of Triton X-100 was increased to 0.1%, and a complete

loss of protease inhibition occurred after incubation with BSA. These findings reinforce the suggested colloidal aggregate behavior of **BR020255**.

**Table 5.** Percentages of ZIKV NS2B-NS3$^{pro}$ activity inhibition by **BR020255** with BSA and different concentrations of Triton X-100.

| BR020255 | % Inhibition [1] with Triton-X | | | % Inhibition [2] with BSA | |
|---|---|---|---|---|---|
| **μM** | **0.001%** | **0.01%** | **0.1%** | **BSA+** | **BSA−** |
| 20 | 16 ± 9 | 31 ± 9 | 14 ± 6 | 2 ± 4 | 16 ± 13 |
| 50 | 100 | 100 | 70 ± 49 | 0 | 100 |

[1] Assays were performed in 10 mM Tris-HCl, 5% *v*/*v* glycerin, and triton X-100 at pH 8.5 in the presence of 9 nM enzyme and 44 μM substrate at 37 °C. [2] The compound was pre-incubated with BSA before the enzyme was added (BSA+). Reported values are represented as the average and standard deviation calculated from two independent assays in triplicate ($n$ = 6 data points).

## 4. Discussion

The ZIKV NS3$^{pro}$ is a well-characterized and studied potential drug target in the search for therapeutic options to treat Zika fever. This protease is essential for the viral cycle, and blocking its activity may abolish the polyprotein cleavage and viral assembly, ceasing viral propagation during the infection. Successful approaches have developed drugs that target different proteases in the past, such as the discovery of boceprevir against hepatitis C virus (HCV) [72], ritonavir against human immunodeficiency virus (HIV) [73], and recently the two SARS-CoV-2 main protease (M$^{pro}$) inhibitors, nirmatrelvir [74] and ensitrelvir [75]. These employed structure-based drug design (SDBB) approaches, such as docking studies, in the design of novel inhibitors. In this sense, cross-studies and docking software validation are important to accurately predict ligand interactions with target residues, as was the case in the design of other protease inhibitors initially designed for SARS-CoV-2 M$^{pro}$, such as boceprevir and GC376 [76,77], and the Michael acceptor inhibitor **N3** [78].

We extensively validated our docking analysis by varying the parameters of GOLD and DockThor (Tables 1 and 2) to a consensus screening of the 1176 compounds from BraCoLi. By this consensus approach, we selected 28 initial hits based on docking scores from the two different software programs, having compounds **BR010385** and **BR010384** predicted with the highest overall scores. Of note, even using appropriate and validated parameters, it is still necessary to perform a visual inspection of the results after docking simulations [79]. This manual step is performed to increase the accuracy of the predicted results by each docking software, as score values alone are dependent on each genetic algorithm and may not be a reliable representative of the ligand structure with the highest affinity for the proposed target [51,79]. In this sense, we characterized the binding site of ZIKV NS3$^{pro}$ using FTSite and PrankWeb (Figure 1), which revealed an overall conserved region with important residues for interaction. These predictions corroborate those previously reported [37], suggesting a hotspot for ligands and potential inhibitors [80].

Then, we analyzed the docking poses for the available remnants **BR020113**, **BR020255**, and **BR020325** before following up with in vitro evaluations. The first two were predicted to have only one or two residue interactions with the ZIKV NS3$^{pro}$, Asn152, and Lys54 and Tyr161, respectively (Figure 2), but not accurately fit into the binding site. Importantly, one should consider that the structural accessibility of a given ligand to the target binding site may be critical to forming a ligand−target complex [81]. Conversely, **BR020325** was predicted to have an interaction with Ser135 (nucleophile), which triggers the proteolytic activity [68] of ZIKV NS3$^{pro}$; thus, it is a desirable feature in an inhibitor.

In our experimental validation assays, **BR020113** and **BR020255** showed less toxicity to Vero cells, with $CC_{50}$ values > 89 μM (i.e., essentially non-toxic), while **BR020325** had

its $CC_{50}$ determined as 29.67 ± 1.01 μM. One could argue that the range of activity for **BR020113** and **BR020255** could be above their $CC_{50}$ values or that they would depend on the ability to permeate the cell membrane [82]. Interestingly, despite the three compounds being structurally different from those available in ChEMBL having anti-ZIKV activities (Figure 4), **BR020325** was the only compound that showed antiviral activity against ZIKV PE243 (SI < 2.37). Low SI values can be an issue for the future application of compounds as lead drug candidates, which ideally should present SI values ≥ 10 [83], such as our inhibition control, ribavirin (SI > 24.39). In this sense, **BR020325** would require further molecular optimization as a potential lead candidate for future anti-ZIKV therapy. To further optimize this compound, structural analogs could be synthesized [70] to increase the antiviral activity [84], such as the addition of hydrophilic substituents (e.g., nitrogen nucleophiles) [85], or decrease cytotoxicity [45,86] while accounting for aqueous solubility and absorption [61] and oral bioavailability [47,55].

Moreover, different anti-ZIKV compounds having a nitro group have shown a higher potential for $NS3^{pro}$ inhibition. In addition, the presence of an azole group was associated with potential antiviral activity in cell-based assays [28]. Among the three selected compounds, **BR020113**, which does not present a nitro group, having a triazole instead, did not show inhibitory activities at tested concentrations in both our experimental assays (Tables 3 and 4). Conversely, **BR020325**, which does not have either nitro or azole groups, displayed ~40% inhibition against ZIKV PE243 at 12.5 μM (Table 3). The interactions that were predicted for this compound (Figure 2C) would be supportive of its potential inhibitory activity to the $NS3^{pro}$, similar to the mechanism suggested for bromocriptine [24], which also interacts with Ser135. However, **BR020325** was also inactive against ZIKV $NS3^{pro}$ up to 100 μM (Table 4). It is important to note that this compound was predicted to have important interactions with the target (Figure 2C), which would support its feasibility of acting as an inhibitor. In this sense, molecular dynamics (MD) simulations could be an additional relevant step to assess ligand-binding stability and the frequencies of interactions of the compounds in the characterized site (Figure 2), supporting the docking simulations and therefore improving the accuracy of our ligand–target predictions [87]. Nevertheless, it is important to consider that differences in the ZIKV NS2B-$NS3^{pro}$ considered for docking simulations (PDB ID: 5YOF), antiviral assays (strain PE243), and the expressed enzyme (strain BeH823339) could interfere with compound interactions and the correlation between our simulations and experimental validations. In this sense, we aligned the sequences, which revealed ~98% identity and no notable substitutions that would impact the binding of inhibitors in the protease active site (Figure S9).

Interestingly, **BR020255**, which was inactive against ZIKV PE243 up to 100 μM (Table 3), displayed an initial inhibitory activity against the $NS3^{pro}$ in our enzymatic inhibition assays and was determined with an $IC_{50}$ of 17 μM (Table 4). However, the high Hill slope observed (Figure S2) led us to further characterize an inhibition likely associated with aggregation behavior (Table 5). This behavior has been suggested as the reason for the loss of protease inhibition depending on assay conditions, such as the addition of detergent [88], and has even been reported for approved drugs at high concentrations [89]. Herein, despite our consensus approach resulting in **BR020325** having antiviral activity (Table 3), its proposed $NS3^{pro}$ inhibition was disregarded (Table 4). Therefore, considering a suggested aggregation mechanism of **BR020255**, it is important to make an educated decision for further validation methods to determine inhibitory activities and mechanisms, especially when considering structurally different compounds and the proposed protease target [71,89,90].

## 5. Conclusions

In the present study, a consensus docking protocol using GOLD and DockThor scores was able to identify potential inhibitors of the ZIKV NS3$^{pro}$. An extensive redocking validation assessed the parameters for a more reliable screening protocol, which resulted in 28 hits initially selected, while three followed experimental validation in vitro. One of the three compounds exhibited antiviral activity in Vero cells infected with ZIKV PE243. Ultimately, we determined their activity against the ZIKV protease, which validated one compound as a colloidal aggregator that inhibited the NS3$^{pro}$. Furthermore, after subsequential structural modifications, the described compounds, having an increased antiviral activity or lower cytotoxicity, might be considered potential lead candidates for future antiviral drug therapy against Zika. Notwithstanding, this consensus approach showed a feasibility for obtaining potential inhibitors with anti-ZIKV activity.

**Supplementary Materials:** The following supporting information can be downloaded at: https://www.mdpi.com/article/10.3390/futurepharmacol5010009/s1, Table S1: Combination of redocking parameters to validate the docking protocol using GOLD. Table S2: Top scored compounds from each docking protocol screened using GOLD (CHEMPLP fitness scores) and DockThor (affinity, in kcal/mol). Figure S1: Docking poses of **BR010385** and **BR010384** to the ZIKV NS3$^{pro}$. Figure S2: Half-maximal inhibitory concentration ($IC_{50}$) curve of compound **BR020255** against ZIKV NS2B-NS3$^{pro}$. Figure S3: $^{1}$H NMR (400 MHz, DMSO-*d*6) spectrum of compound **BR020113**. Figure S4: $^{13}$C and DEPT-135 NMR (100 MHz, DMSO-*d*6) spectra of compound **BR020113**. Figure S5: $^{1}$H NMR (600 MHz, $CDCl_3$) spectrum of compound **BR020325**. Figure S6: Expansion of the $^{1}$H NMR (600 MHz, $CDCl_3$) spectrum of compound **BR020325**. Figure S7: $^{13}$C and DEPT-135 NMR (100 MHz, DMSO-*d*6) spectra of compound BR020325. Figure S8: UHPLC chromatogram and HRMS (ESI) spectrum (UHPLC-HRMS/MS) of compound **BR020113**. Figure S9: Alignment of the ZIKV NS2B-NS3$^{pro}$ sequences.

**Author Contributions:** Conceptualization, M.S.M.S.; methodology, B.M.R.M.R., E.G.d.O., F.K.M.e.O., M.M.S.A.V., M.S.M.S., R.B.d.O., V.G.M., and T.K.; software, M.S.M.S., V.G.M., and T.K.; validation, B.M.R.M.R., E.G.d.O., F.K.M.e.O., M.S.M.S., and T.K.; formal analysis, B.M.R.M.R., E.G.d.O., F.K.M.e.O., M.M.S.A.V., M.S.M.S., R.B.d.O., R.J.A., R.S.F., and T.K.; investigation, B.M.R.M.R., F.K.M.e.O., M.M.S.A.V., M.S.M.S., R.B.d.O., R.J.A., V.G.M., and T.K.; resources, J.S.A., R.B.d.O., R.J.A., R.S.F., V.G.M., and T.K.; data curation, M.S.M.S., R.S.F., and T.K.; writing—original draft preparation, F.K.M.e.O., E.G.d.O., and M.S.M.S.; writing—review and editing, B.M.R.M.R., E.G.d.O., F.K.M.e.O., M.S.M.S., V.G.M., R.S.F., and T.K.; visualization, F.K.M.e.O., J.S.A., M.M.S.A.V., M.S.M.S., R.B.d.O., and R.J.A.; supervision, J.S.A., M.S.M.S., R.J.A., and R.S.F.; project administration, J.S.A., M.S.M.S., and R.J.A.; funding acquisition, J.S.A., M.S.M.S., R.B.d.O., R.J.A., R.S.F., V.G.M., and T.K. All authors have read and agreed to the published version of the manuscript.

**Funding:** This research was funded by Coordenação de Aperfeiçoamento de Pessoal de Ensino Superior (CAPES), grant number 88887.664178/2022-00; Conselho Nacional de Desenvolvimento Científico e Tecnológico (CNPq), grant number 152673/2024-5; Fundação de Amparo à Pesquisa do Estado de Minas Gerais (FAPEMIG), grant numbers BPD-00076-22, APQ-01818-21, APQ-00789-22, and REDE-00110-23; and UFMG intramural funds. J.S.A., R.B.d.O., and R.S.F. are researchers awarded with CNPq Productivity Scholarship. T.K. is funded by the German Center for Infection Research (DZIF, TTU06.716).

**Institutional Review Board Statement:** Not applicable.

**Informed Consent Statement:** Not applicable.

**Data Availability Statement:** The redocking and docking results are available in the Zenodo repository (under the codes: 10.5281/zenodo.14531461). BraCoLi compounds are publicly available at https://www.farmacia.ufmg.br/qf/downloads/ (accessed on 4 February 2024).

**Acknowledgments:** The authors would like to thank OpenEye Scientific Software (Cadence Molecular Sciences) for the academic licenses and the CSC—Finland for the generous computational resources provided. The authors would also like to thank UFMG for intramural funds and express their gratitude to the Laboratório de Ressonância Magnética Nuclear de Alta Resolução (LAREMAR) at UFMG for their collaboration in obtaining the NMR spectra. The authors also thank Rafael Eduardo Oliveira Rocha for the previous expression and purification of the ZIKV enzyme. M.S.M.S. thanks to his PDJ scholarship from CNPq (152673/2024-5). All authors agree with the declared acknowledgments.

**Conflicts of Interest:** The authors declare no conflicts of interest.

## References

1. Postler, T.S.; Beer, M.; Blitvich, B.J.; Bukh, J.; de Lamballerie, X.; Drexler, J.F.; Imrie, A.; Kapoor, A.; Karganova, G.G.; Lemey, P.; et al. Renaming of the Genus Flavivirus to Orthoflavivirus and Extension of Binomial Species Names within the Family Flaviviridae. *Arch. Virol.* **2023**, *168*, 224. [CrossRef] [PubMed]
2. Baud, D.; Gubler, D.J.; Schaub, B.; Lanteri, M.C.; Musso, D. An Update on Zika Virus Infection. *Lancet* **2017**, *390*, 2099–2109. [CrossRef]
3. Pierson, T.C.; Diamond, M.S. The Continued Threat of Emerging Flaviviruses. *Nat. Microbiol.* **2020**, *5*, 796–812. [CrossRef] [PubMed]
4. Boyer, S.; Calvez, E.; Chouin-Carneiro, T.; Diallo, D.; Failloux, A.-B. An Overview of Mosquito Vectors of Zika Virus. *Microbes Infect.* **2018**, *20*, 646–660. [CrossRef]
5. Bisia, M.; Montenegro-Quinoñez, C.A.; Dambach, P.; Deckert, A.; Horstick, O.; Kolimenakis, A.; Louis, V.R.; Manrique-Saide, P.; Michaelakis, A.; Runge-Ranzinger, S.; et al. Secondary Vectors of Zika Virus, a Systematic Review of Laboratory Vector Competence Studies. *PLoS Neglect. Trop. Dis.* **2023**, *17*, e0011591. [CrossRef] [PubMed]
6. Neufeldt, C.J.; Cortese, M.; Acosta, E.G.; Bartenschlager, R. Rewiring Cellular Networks by Members of the Flaviviridae Family. *Nat. Rev. Microbiol.* **2018**, *16*, 125–142. [CrossRef] [PubMed]
7. Ferraris, P.; Yssel, H.; Missé, D. Zika Virus Infection: An Update. *Microbes Infect.* **2019**, *21*, 353–360. [CrossRef] [PubMed]
8. Adachi, A.; Shabbir, M.Z.; Negrete, O.; Singh, R.K.; Dhama, K.; Hmn, I.; Karthik, K.; Tiwari, R.; Khandia, R.; Munjal, A.; et al. Advances in Diagnosis, Surveillance, and Monitoring of Zika Virus: An Update. *Front. Microbiol.* **2018**, *8*, 2677. [CrossRef]
9. Peiter, P.C.; Pereira, R.d.S.; Nunes Moreira, M.C.; Nascimento, M.; Tavares, M.d.F.L.; Franco, V.d.C.; Carvajal Cortês, J.J.; Campos, D.d.S.; Barcellos, C. Zika Epidemic and Microcephaly in Brazil: Challenges for Access to Health Care and Promotion in Three Epidemic Areas. *PLoS ONE* **2020**, *15*, e0235010. [CrossRef] [PubMed]
10. França, G.V.A.; Schuler-Faccini, L.; Oliveira, W.K.; Henriques, C.M.P.; Carmo, E.H.; Pedi, V.D.; Nunes, M.L.; Castro, M.C.; Serruya, S.; Silveira, M.F.; et al. Congenital Zika Virus Syndrome in Brazil: A Case Series of the First 1501 Livebirths with Complete Investigation. *Lancet* **2016**, *388*, 891–897. [CrossRef] [PubMed]
11. Mlakar, J.; Korva, M.; Tul, N.; Popović, M.; Poljšak-Prijatelj, M.; Mraz, J.; Kolenc, M.; Resman Rus, K.; Vesnaver Vipotnik, T.; Fabjan Vodušek, V.; et al. Zika Virus Associated with Microcephaly. *N. Engl. J. Med.* **2016**, *374*, 951–958. [CrossRef] [PubMed]
12. Parra, B.; Lizarazo, J.; Jiménez-Arango, J.A.; Zea-Vera, A.F.; González-Manrique, G.; Vargas, J.; Angarita, J.A.; Zuñiga, G.; Lopez-Gonzalez, R.; Beltran, C.L.; et al. Guillain–Barré Syndrome Associated with Zika Virus Infection in Colombia. *N. Engl. J. Med.* **2016**, *375*, 1513–1523. [CrossRef] [PubMed]
13. Davies, A.J.; Lleixà, C.; Siles, A.M.; Gourlay, D.S.; Berridge, G.; Dejnirattisai, W.; Ramírez-Santana, C.; Anaya, J.-M.; Falconar, A.K.; Romero-Vivas, C.M.; et al. Guillain-Barré Syndrome Following Zika Virus Infection Is Associated With a Diverse Spectrum of Peripheral Nerve Reactive Antibodies. *Neurol. Neuroimmunol. Neuroinflamm.* **2023**, *10*, e200047. [CrossRef] [PubMed]
14. McCarthy, N.; Giesecke, J. Incidence of Guillain-Barré Syndrome Following Infection with Campylobacter Jejuni. *Am. J. Epidemiol.* **2001**, *153*, 610–614. [CrossRef] [PubMed]
15. Nyati, K.K.; Nyati, R. Role of Campylobacter Jejuni Infection in the Pathogenesis of Guillain-Barré Syndrome: An Update. *BioMed Res. Int.* **2013**, *2013*, 852195. [CrossRef]
16. Lynch, R.M.; Mantus, G.; Encinales, L.; Pacheco, N.; Li, G.; Porras, A.; Mendoza, A.R.; Peng, J.; Rengifo-Pardo, M.; Cruz, M.M.; et al. Augmented Zika and Dengue Neutralizing Antibodies Are Associated With Guillain-Barré Syndrome. *J. Infect. Dis.* **2019**, *219*, 26–30. [CrossRef] [PubMed]
17. Pattnaik, A.; Sahoo, B.R.; Pattnaik, A.K. Current Status of Zika Virus Vaccines: Successes and Challenges. *Vaccines* **2020**, *8*, 266. [CrossRef] [PubMed]
18. Peng, Z.-Y.; Yang, S.; Lu, H.-Z.; Wang, L.-M.; Li, N.; Zhang, H.-T.; Xing, S.-Y.; Du, Y.-N.; Deng, S.-Q. A Review on Zika Vaccine Development. *Pathog. Dis.* **2024**, *82*, ftad036. [CrossRef] [PubMed]
19. Tayal, A.; Kabra, S.K.; Lodha, R. Management of Dengue: An Updated Review. *Indian. J. Pediatr.* **2023**, *90*, 168–177. [CrossRef]

20. Baz, M.; Boivin, G. Antiviral Agents in Development for Zika Virus Infections. *Pharmaceuticals* **2019**, *12*, 101. [CrossRef] [PubMed]
21. Bifani, A.M.; Chan, K.W.K.; Borrenberghs, D.; Tan, M.J.A.; Phoo, W.W.; Watanabe, S.; Goethals, O.; Vasudevan, S.G.; Choy, M.M. Therapeutics for Flaviviral Infections. *Antivir. Res.* **2023**, *210*, 105517. [CrossRef] [PubMed]
22. Kang, C.; Keller, T.H.; Luo, D. Zika Virus Protease: An Antiviral Drug Target. *Trends Microbiol.* **2017**, *25*, 797–808. [CrossRef] [PubMed]
23. Lei, J.; Hansen, G.; Nitsche, C.; Klein, C.D.; Zhang, L.; Hilgenfeld, R. Crystal Structure of Zika Virus NS2B-NS3 Protease in Complex with a Boronate Inhibitor. *Science* **2016**, *353*, 503–505. [CrossRef] [PubMed]
24. Chan, J.F.W.; Chik, K.K.H.; Yuan, S.; Yip, C.C.Y.; Zhu, Z.; Tee, K.M.; Tsang, J.O.L.; Chan, C.C.S.; Poon, V.K.M.; Lu, G.; et al. Novel Antiviral Activity and Mechanism of Bromocriptine as a Zika Virus NS2B-NS3 Protease Inhibitor. *Antivir. Res.* **2017**, *141*, 29–37. [CrossRef]
25. Li, Y.; Zhang, Z.; Phoo, W.W.; Loh, Y.R.; Li, R.; Yang, H.Y.; Jansson, A.E.; Hill, J.; Keller, T.H.; Nacro, K.; et al. Structural Insights into the Inhibition of Zika Virus NS2B-NS3 Protease by a Small-Molecule Inhibitor. *Structure* **2018**, *26*, 555–564.e3. [CrossRef] [PubMed]
26. da Silva-Júnior, E.F.; de Araújo-Júnior, J.X. Peptide Derivatives as Inhibitors of NS2B-NS3 Protease from Dengue, West Nile, and Zika Flaviviruses. *Bioorg. Med. Chem.* **2019**, *27*, 3963–3978. [CrossRef] [PubMed]
27. Serafim, M.S.M.; Dos Santos Júnior, V.S.; Gertrudes, J.C.; Maltarollo, V.G.; Honorio, K.M. Machine Learning Techniques Applied to the Drug Design and Discovery of New Antivirals: A Brief Look over the Past Decade. *Expert Opin. Drug Discov.* **2021**, *16*, 961–975. [CrossRef] [PubMed]
28. Nunes, D.A.d.F.; Santos, F.R.d.S.; da Fonseca, S.T.D.; de Lima, W.G.; Nizer, W.S.d.C.; Ferreira, J.M.S.; de Magalhães, J.C. NS2B-NS3 Protease Inhibitors as Promising Compounds in the Development of Antivirals against Zika Virus: A Systematic Review. *J. Med. Virol.* **2022**, *94*, 442–453. [CrossRef]
29. Mirza, M.U.; Alanko, I.; Vanmeert, M.; Muzzarelli, K.M.; Salo-Ahen, O.M.H.; Abdullah, I.; Kovari, I.A.; Claes, S.; De Jonghe, S.; Schols, D.; et al. The Discovery of Zika Virus NS2B-NS3 Inhibitors with Antiviral Activity via an Integrated Virtual Screening Approach. *Eur. J. Pharm. Sci.* **2022**, *175*, 106220. [CrossRef] [PubMed]
30. Lin, W.-W.; Huang, Y.-J.; Wang, Y.-T.; Lin, Y.-S.; Mazibuko, N.; Chen, C.-S.; Cheng, T.-L.; Chang, C.-S.; Leu, Y.-L.; Chen, C.-Y.; et al. Development of NS2B-NS3 Protease Inhibitor That Impairs Zika Virus Replication. *Virus Res.* **2023**, *329*, 199092. [CrossRef] [PubMed]
31. Sadybekov, A.V.; Katritch, V. Computational Approaches Streamlining Drug Discovery. *Nature* **2023**, *616*, 673–685. [CrossRef] [PubMed]
32. Shiryaev, S.A.; Farhy, C.; Pinto, A.; Huang, C.-T.; Simonetti, N.; Ngono, A.E.; Dewing, A.; Shresta, S.; Pinkerton, A.B.; Cieplak, P.; et al. Characterization of the Zika Virus Two-Component NS2B-NS3 Protease and Structure-Assisted Identification of Allosteric Small-Molecule Antagonists. *Antivir. Res.* **2017**, *143*, 218–229. [CrossRef] [PubMed]
33. Brecher, M.; Li, Z.; Liu, B.; Zhang, J.; Koetzner, C.A.; Alifarag, A.; Jones, S.A.; Lin, Q.; Kramer, L.D.; Li, H. A Conformational Switch High-Throughput Screening Assay and Allosteric Inhibition of the Flavivirus NS2B-NS3 Protease. *PLoS Pathog.* **2017**, *13*, e1006411. [CrossRef] [PubMed]
34. Lee, H.; Ren, J.; Nocadello, S.; Rice, A.J.; Ojeda, I.; Light, S.; Minasov, G.; Vargas, J.; Nagarathnam, D.; Anderson, W.F.; et al. Identification of Novel Small Molecule Inhibitors against NS2B/NS3 Serine Protease from Zika Virus. *Antivir. Res.* **2017**, *139*, 49–58. [CrossRef]
35. Yao, Y.; Huo, T.; Lin, Y.-L.; Nie, S.; Wu, F.; Hua, Y.; Wu, J.; Kneubehl, A.R.; Vogt, M.B.; Rico-Hesse, R.; et al. Discovery, X-Ray Crystallography and Antiviral Activity of Allosteric Inhibitors of Flavivirus NS2B-NS3 Protease. *J. Am. Chem. Soc.* **2019**, *141*, 6832–6836. [CrossRef] [PubMed]
36. Santos, L.H.; Rocha, R.E.O.; Dias, D.L.; Ribeiro, B.M.R.M.; Serafim, M.S.M.; Abrahão, J.S.; Ferreira, R.S. Evaluating Known Zika Virus NS2B-NS3 Protease Inhibitor Scaffolds via In Silico Screening and Biochemical Assays. *Pharmaceuticals* **2023**, *16*, 1319. [CrossRef] [PubMed]
37. Serafim, M.S.M.; Kronenberger, T.; Rocha, R.E.O.; Rosa, A.D.R.A.; Mello, T.L.G.; Poso, A.; Ferreira, R.S.; Abrahão, J.S.; Kroon, E.G.; Mota, B.E.F.; et al. Aminopyrimidine Derivatives as Multiflavivirus Antiviral Compounds Identified from a Consensus Virtual Screening Approach. *J. Chem. Inf. Model.* **2024**, *64*, 393–411. [CrossRef] [PubMed]
38. Andrade, M.A.; Mottin, M.; Sousa, B.K.d.P.; Barbosa, J.A.R.G.; dos Santos Azevedo, C.; Lasse Silva, C.; Gonçalves de Andrade, M.; Motta, F.N.; Maulay-Bailly, C.; Amand, S.; et al. Identification of Novel Zika Virus NS3 Protease Inhibitors with Different Inhibition Modes by Integrative Experimental and Computational Approaches. *Biochimie* **2023**, *212*, 143–152. [CrossRef] [PubMed]
39. Yuan, S.; Chan, J.F.W.; den-Haan, H.; Chik, K.K.H.; Zhang, A.J.; Chan, C.C.S.; Poon, V.K.M.; Yip, C.C.Y.; Mak, W.W.N.; Zhu, Z.; et al. Structure-Based Discovery of Clinically Approved Drugs as Zika Virus NS2B-NS3 Protease Inhibitors That Potently Inhibit Zika Virus Infection in Vitro and in Vivo. *Antivir. Res.* **2017**, *145*, 33–43. [CrossRef] [PubMed]
40. Houston, D.R.; Walkinshaw, M.D. Consensus Docking: Improving the Reliability of Docking in a Virtual Screening Context. *J. Chem. Inf. Model.* **2013**, *53*, 384–390. [CrossRef]

41. Blanes-Mira, C.; Fernández-Aguado, P.; de Andrés-López, J.; Fernández-Carvajal, A.; Ferrer-Montiel, A.; Fernández-Ballester, G. Comprehensive Survey of Consensus Docking for High-Throughput Virtual Screening. *Molecules* **2023**, *28*, 175. [CrossRef] [PubMed]
42. Lavorato, S.N.; Sales Júnior, P.A.; Murta, S.M.F.; Romanha, A.J.; Alves/, R.J. In Vitro Activity of 1,3-Bisaryloxypropanamines against *Trypanosoma Cruzi*-Infected L929 Cultures. *Mem. Inst. Oswaldo Cruz* **2015**, *110*, 566–568. [CrossRef] [PubMed]
43. Lavorato, S.N.; Duarte, M.C.; Lage, D.P.; Tavares, C.A.P.; Coelho, E.A.F.; Alves, R.J. Synthesis and Antileishmanial Activity of 1,3-Bis(Aryloxy)Propan-2-Amines. *Med. Chem. Res.* **2017**, *26*, 1052–1072. [CrossRef]
44. Lavorato, S.N.; Duarte, M.C.; Lage, D.P.; Tavares, C.A.P.; Coelho, E.A.F.; Alves, R.J. 1,3-Bis(Aryloxy)Propan-2-Ols as Potential Antileishmanial Agents. *Chem. Biol. Drug Des.* **2017**, *90*, 981–986. [CrossRef] [PubMed]
45. Serafim, M.S.M.; Lavorato, S.N.; Kronenberger, T.; Sousa, Y.V.; Oliveira, G.P.; Dos Santos, S.G.; Kroon, E.G.; Maltarollo, V.G.; Alves, R.J.; Mota, B.E.F. Antibacterial Activity of Synthetic 1,3-Bis(Aryloxy)Propan-2-Amines against Gram-Positive Bacteria. *Microbiologyopen* **2019**, *8*, e814. [CrossRef]
46. Maltarollo, V.G.; da Silva, E.B.; Kronenberger, T.; Sena Andrade, M.M.; de Lima Marques, G.V.; Cândido Oliveira, N.J.; Santos, L.H.; Oliveira Rezende Júnior, C.d.; Cassiano Martinho, A.C.; Skinner, D.; et al. Structure-Based Discovery of Thiosemicarbazones as SARS-CoV-2 Main Protease Inhibitors. *Future Med. Chem.* **2023**, *15*, 959–985. [CrossRef] [PubMed]
47. Fernandes, P.O.; Dias, A.L.T.; dos Santos Júnior, V.S.; Sá Magalhães Serafim, M.; Sousa, Y.V.; Monteiro, G.C.; Coutinho, I.D.; Valli, M.; Verzola, M.M.S.A.; Ottoni, F.M.; et al. Machine Learning-Based Virtual Screening of Antibacterial Agents against Methicillin-Susceptible and Resistant Staphylococcus Aureus. *J. Chem. Inf. Model.* **2024**, *64*, 1932–1944. [CrossRef] [PubMed]
48. Andrad, S.F.; Campos, E.F.S.; Teixeira, C.S.; Bandeira, C.C.; Lavorato, S.N.; Romeiro, N.C.; Bertollo, C.M.; Oliveira, M.C.; Souza-Fagundes, E.M.; Alves, R.J. Synthesis of Novel 2,3,4-Trisubstituted-Oxazolidine Derivatives and in Vitro Cytotoxic Evaluation. *Med. Chem.* **2014**, *10*, 609–618. [CrossRef] [PubMed]
49. Santana, P.A.L.; Andrade, M.M.S.; Marques, G.V.d.L.; Evangelista, F.C.G.; Freitas, T.R.; Sabino, A.d.P.; Oliveira, R.B. de Síntese e avaliação de potencial atividade antitumoral de derivados arilfuranos / Synthesis and evaluation of potential antitumor activity of arylfuran derivatives. *Braz. J. Health Rev.* **2022**, *5*, 9318–9324. [CrossRef]
50. Veríssimo, G.C.; Dos Santos Júnior, V.S.; de Almeida, I.A.d.R.; Ruas, M.S.M.; Coutinho, L.G.; de Oliveira, R.B.; Alves, R.J.; Maltarollo, V.G. The Brazilian Compound Library (BraCoLi) Database: A Repository of Chemical and Biological Information for Drug Design. *Mol. Divers.* **2022**, *26*, 3387–3397. [CrossRef]
51. Azevedo, L.; Serafim, M.S.M.; Maltarollo, V.G.; Grabrucker, A.M.; Granato, D. Atherosclerosis Fate in the Era of Tailored Functional Foods: Evidence-Based Guidelines Elicited from Structure- and Ligand-Based Approaches. *Trends Food Sci. Technol.* **2022**, *128*, 75–89. [CrossRef]
52. Vallone, A.; D'Alessandro, S.; Brogi, S.; Brindisi, M.; Chemi, G.; Alfano, G.; Lamponi, S.; Lee, S.G.; Jez, J.M.; Koolen, K.J.M.; et al. Antimalarial Agents against Both Sexual and Asexual Parasites Stages: Structure-Activity Relationships and Biological Studies of the Malaria Box Compound 1-[5-(4-Bromo-2-Chlorophenyl)Furan-2-Yl]- N -[(Piperidin-4-Yl)Methyl]Methanamine (MMV019918) and Analogues. *Eur. J. Med. Chem.* **2018**, *150*, 698–718. [CrossRef] [PubMed]
53. Verdonk, M.L.; Cole, J.C.; Hartshorn, M.J.; Murray, C.W.; Taylor, R.D. Improved Protein-Ligand Docking Using GOLD. *Proteins: Struct. Funct. Genet.* **2003**, *52*, 609–623. [CrossRef] [PubMed]
54. Guedes, I.A.; Pereira da Silva, M.M.; Galheigo, M.; Krempser, E.; de Magalhães, C.S.; Correa Barbosa, H.J.; Dardenne, L.E. DockThor-VS: A Free Platform for Receptor-Ligand Virtual Screening. *J. Mol. Biol.* **2024**, *436*, 168548. [CrossRef] [PubMed]
55. Liu, L.J.; Francisco, K.R.; Sun, Y.U.; Serafim, M.S.M.; Amarasinghe, D.K.; Teixeira, T.R.; Lucero, B.; Kronenberger, T.; Elsayed, W.; Elwakeel, H.; et al. Carmaphycin B-Based Proteasome Inhibitors to Treat Human African Trypanosomiasis: Structure–Activity Relationship and In Vivo Efficacy. *ACS Infect. Dis.* **2024**, *12*, 4182–4193. [CrossRef]
56. Gaulton, A.; Hersey, A.; Nowotka, M.; Bento, A.P.; Chambers, J.; Mendez, D.; Mutowo, P.; Atkinson, F.; Bellis, L.J.; Cibrián-Uhalte, E.; et al. The ChEMBL Database in 2017. *Nucleic Acids Res* **2017**, *45*, D945–D954. [CrossRef] [PubMed]
57. Landrum, G. RDKit Documentation. *Open Source Toolkit Cheminformatics*. 2019. RDKit: Open-source cheminformatics (2024.09.5 documentation). Available online: https://www.rdkit.org (accessed on 23 November 2024).
58. Berthold, M.R.; Cebron, N.; Dill, F.; Gabriel, T.R.; Kötter, T.; Meinl, T.; Ohl, P.; Sieb, C.; Thiel, K.; Wiswedel, B. KNIME: The Konstanz Information Miner. In *Data Analysis, Machine Learning and Applications*; Preisach, C., Burkhardt, H., Schmidt-Thieme, L., Decker, R., Eds.; Studies in Classification, Data Analysis, and Knowledge Organization; Springer: Berlin/Heidelberg, Germany, 2008; pp. 319–326. ISBN 978-3-540-78239-1.
59. Andrade, M.M.S.; Protti, Í.F.; Maltarollo, V.G.; da Costa, Y.F.G.; de Moraes, W.G.; Moreira, N.F.; Garcia, G.G.; Caran, G.F.; Ottoni, F.M.; Alves, R.J.; et al. Synthesis of Arylfuran Derivatives as Potential Antibacterial Agents. *Med. Chem. Res.* **2021**, *30*, 1074–1086. [CrossRef]
60. Donald, C.L.; Brennan, B.; Cumberworth, S.L.; Rezelj, V.V.; Clark, J.J.; Cordeiro, M.T.; França, R.F.d.O.; Pena, L.J.; Wilkie, G.S.; Filipe, A.D.S.; et al. Full Genome Sequence and sfRNA Interferon Antagonist Activity of Zika Virus from Recife, Brazil. *PLoS Neglect. Trop. Dis.* **2016**, *10*, e0005048. [CrossRef] [PubMed]

61. Serafim, M.S.M.; Kronenberger, T.; de Oliveira, R.B.; Kroon, E.G.; Abrahão, J.S.; Mota, B.E.F.; Maltarollo, V.G. Synthetic Curcumin Analogues Present Antiflavivirus Activity In Vitro with Potential Multiflavivirus Activity from a Thiazolylhydrazone Moiety. *Future Pharmacol.* **2023**, *3*, 364–378. [CrossRef]
62. Mosmann, T. Rapid Colorimetric Assay for Cellular Growth and Survival: Application to Proliferation and Cytotoxicity Assays. *J. Immunol. Methods* **1983**, *65*, 55–63. [CrossRef] [PubMed]
63. Takeuchi, H.; Baba, M.; Shigeta, S. An Application of Tetrazolium (MTT) Colorimetric Assay for the Screening of Anti-Herpes Simplex Virus Compounds. *J. Virol. Methods* **1991**, *33*, 61–71. [CrossRef]
64. Dias, R.F.C.; Ribeiro, B.M.R.M.; Cassani, N.M.; Farago, D.N.; Antoniucci, G.A.; de Oliveira Rocha, R.E.; de Oliveira Souza, F.; Pilau, E.J.; Jardim, A.C.G.; Ferreira, R.S.; et al. Discovery and Structural Optimization of a New Series of *N*-Acyl-2-Aminobenzothiazole as Inhibitors of Zika Virus. *Bioorg. Med. Chem.* **2023**, *95*, 117488. [CrossRef]
65. Sapundzhi, F.; Prodanova, K.; Lazarova, M. Survey of the Scoring Functions for Protein-Ligand Docking. *AIP Conf. Proc.* **2019**, *2172*, 100008. [CrossRef]
66. Korb, O.; Stützle, T.; Exner, T.E. Empirical Scoring Functions for Advanced Protein−Ligand Docking with PLANTS. *J. Chem. Inf. Model.* **2009**, *49*, 84–96. [CrossRef] [PubMed]
67. Sapundzhi, F.; Dzimbova, T.; Pencheva, N.; Milanov, P. GOLD Scoring Functions Comparison to Establish the Relationship Structure-Biological Action. *J. Pept. Sci.* **2014**, *20*, S294–S295.
68. Timiri, A.K.; Sinha, B.N.; Jayaprakash, V. Progress and Prospects on DENV Protease Inhibitors. *Eur. J. Med. Chem.* **2016**, *117*, 125–143. [CrossRef] [PubMed]
69. de Oliveira, R.B.; de Souza-Fagundes, E.M.; Siqueira, H.A.J.; Leite, R.S.; Donnici, C.L.; Zani, C.L. Synthesis and Evaluation of Cytotoxic Activity of Arylfurans. *Eur. J. Med. Chem.* **2006**, *41*, 756–760. [CrossRef] [PubMed]
70. Hendrix, M.; Alper, P.B.; Priestley, E.S.; Wong, C.-H. Hydroxyamines as a New Motif for the Molecular Recognition of Phosphodiesters: Implications for Aminoglycoside–RNA Interactions. *Angew. Chem. Int. Ed. Engl.* **1997**, *36*, 95–98. [CrossRef]
71. Jadhav, A.; Ferreira, R.S.; Klumpp, C.; Mott, B.T.; Austin, C.P.; Inglese, J.; Thomas, C.J.; Maloney, D.J.; Shoichet, B.K.; Simeonov, A. Quantitative Analyses of Aggregation, Autofluorescence, and Reactivity Artifacts in a Screen for Inhibitors of a Thiol Protease. *J. Med. Chem.* **2010**, *53*, 37–51. [CrossRef] [PubMed]
72. Njoroge, F.G.; Chen, K.X.; Shih, N.-Y.; Piwinski, J.J. Challenges in Modern Drug Discovery: A Case Study of Boceprevir, an HCV Protease Inhibitor for the Treatment of Hepatitis C Virus Infection. *Acc. Chem. Res.* **2008**, *41*, 50–59. [CrossRef] [PubMed]
73. De Clercq, E. Anti-HIV Drugs: 25 Compounds Approved within 25 Years after the Discovery of HIV. *Int. J. Antimicrob. Agents* **2009**, *33*, 307–320. [CrossRef] [PubMed]
74. Hoffman, R.L.; Kania, R.S.; Brothers, M.A.; Davies, J.F.; Ferre, R.A.; Gajiwala, K.S.; He, M.; Hogan, R.J.; Kozminski, K.; Li, L.Y.; et al. Discovery of Ketone-Based Covalent Inhibitors of Coronavirus 3CL Proteases for the Potential Therapeutic Treatment of COVID-19. *J. Med. Chem.* **2020**, *63*, 12725–12747. [CrossRef]
75. Unoh, Y.; Uehara, S.; Nakahara, K.; Nobori, H.; Yamatsu, Y.; Yamamoto, S.; Maruyama, Y.; Taoda, Y.; Kasamatsu, K.; Suto, T.; et al. Discovery of S-217622, a Noncovalent Oral SARS-CoV-2 3CL Protease Inhibitor Clinical Candidate for Treating COVID-19. *J. Med. Chem.* **2022**, *65*, 6499–6512. [CrossRef]
76. Fu, L.; Ye, F.; Feng, Y.; Yu, F.; Wang, Q.; Wu, Y.; Zhao, C.; Sun, H.; Huang, B.; Niu, P.; et al. Both Boceprevir and GC376 Efficaciously Inhibit SARS-CoV-2 by Targeting Its Main Protease. *Nat. Commun.* **2020**, *11*, 4417. [CrossRef] [PubMed]
77. Ma, C.; Sacco, M.D.; Hurst, B.; Townsend, J.A.; Hu, Y.; Szeto, T.; Zhang, X.; Tarbet, B.; Marty, M.T.; Chen, Y.; et al. Boceprevir, GC-376, and Calpain Inhibitors II, XII Inhibit SARS-CoV-2 Viral Replication by Targeting the Viral Main Protease. *Cell Res.* **2020**, *30*, 678–692. [CrossRef] [PubMed]
78. Jin, Z.; Du, X.; Xu, Y.; Deng, Y.; Liu, M.; Zhao, Y.; Zhang, B.; Li, X.; Zhang, L.; Peng, C.; et al. Structure of Mpro from SARS-CoV-2 and Discovery of Its Inhibitors. *Nature* **2020**, *582*, 289–293. [CrossRef]
79. Fischer, A.; Smieško, M.; Sellner, M.; Lill, M.A. Decision Making in Structure-Based Drug Discovery: Visual Inspection of Docking Results. *J. Med. Chem.* **2021**, *64*, 2489–2500. [CrossRef] [PubMed]
80. Barillari, C.; Marcou, G.; Rognan, D. Hot-Spots-Guided Receptor-Based Pharmacophores (HS-Pharm): A Knowledge-Based Approach to Identify Ligand-Anchoring Atoms in Protein Cavities and Prioritize Structure-Based Pharmacophores. *J. Chem. Inf. Model.* **2008**, *48*, 1396–1410. [CrossRef] [PubMed]
81. Aleshin, A.E.; Shiryaev, S.A.; Strongin, A.Y.; Liddington, R.C. Structural Evidence for Regulation and Specificity of Flaviviral Proteases and Evolution of the Flaviviridae Fold. *Protein Sci.* **2007**, *16*, 795–806. [CrossRef] [PubMed]
82. Bennion, B.J.; Be, N.A.; McNerney, M.W.; Lao, V.; Carlson, E.M.; Valdez, C.A.; Malfatti, M.A.; Enright, H.A.; Nguyen, T.H.; Lightstone, F.C.; et al. Predicting a Drug's Membrane Permeability: A Computational Model Validated With in Vitro Permeability Assay Data. *J. Phys. Chem. B* **2017**, *121*, 5228–5237. [CrossRef] [PubMed]
83. Tuberculosis Drug Screening Program, T.D.S. Search for New Drugs for Treatment of Tuberculosis. *Antimicrob. Agents Chemother.* **2001**, *45*, 1943. [CrossRef]

84. Yusufzai, S.K.; Osman, H.; Khan, M.S.; Razik, B.M.A.; Mohamad, S.; Sulaiman, O.; Gansau, J.A.; Johansah, N.; Ezzat, M.O.; Parumasivam, T.; et al. Synthesis, X-Ray Crystallographic Study, Pharmacology and Docking of Hydrazinyl Thiazolyl Coumarins as Dengue Virus NS2B/NS3 Serine Protease Inhibitors. *Med. Chem. Res.* **2018**, *27*, 1647–1665. [CrossRef]
85. Pu, S.-Y.; Wouters, R.; Schor, S.; Rozenski, J.; Barouch-Bentov, R.; Prugar, L.I.; O'Brien, C.M.; Brannan, J.M.; Dye, J.M.; Herdewijn, P.; et al. Optimization of Isothiazolo[4,3-b]Pyridine-Based Inhibitors of Cyclin G Associated Kinase (GAK) with Broad-Spectrum Antiviral Activity. *J. Med. Chem.* **2018**, *61*, 6178–6192. [CrossRef] [PubMed]
86. Wiji Prasetyaningrum, P.; Bahtiar, A.; Hayun, H. Synthesis and Cytotoxicity Evaluation of Novel Asymmetrical Mono-Carbonyl Analogs of Curcumin (AMACs) against Vero, HeLa, and MCF7 Cell Lines. *Sci. Pharm.* **2018**, *86*, 25. [CrossRef]
87. Santos, L.H.S.; Ferreira, R.S.; Caffarena, E.R. Integrating Molecular Docking and Molecular Dynamics Simulations. In *Docking Screens for Drug Discovery*; de Azevedo, W.F., Jr., Ed.; Methods in Molecular Biology; Springer: Berlin/Heidelberg, Germany, 2019; pp. 13–34. ISBN 978-1-4939-9752-7.
88. Yildiz, M.; Ghosh, S.; Bell, J.A.; Sherman, W.; Hardy, J.A. Allosteric Inhibition of the NS2B-NS3 Protease from Dengue Virus. *ACS Chem. Biol.* **2013**, *8*, 2744–2752. [CrossRef] [PubMed]
89. Seidler, J.; McGovern, S.L.; Doman, T.N.; Shoichet, B.K. Identification and Prediction of Promiscuous Aggregating Inhibitors among Known Drugs. *J. Med. Chem.* **2003**, *46*, 4477–4486. [CrossRef] [PubMed]
90. Simeonov, A.; Jadhav, A.; Thomas, C.J.; Wang, Y.; Huang, R.; Southall, N.T.; Shinn, P.; Smith, J.; Austin, C.P.; Auld, D.S.; et al. Fluorescence Spectroscopic Profiling of Compound Libraries. *J. Med. Chem.* **2008**, *51*, 2363–2371. [CrossRef]